THE ASTROPHYSICAL JOURNAL, 387:372–393, 1992 March 1

STANDARD SOLAR MODEL

D. B. GUENTHER, P. DEMARQUE, Y.-C. KIM, AND M. H. PINSONNEAULT
Center for Solar and Space Research, Department of Astronomy, Yale University, P.O. Box 6666, New Haven, CT 06511
Received 1991 June 3; accepted 1991 August 29

ABSTRACT

A set of solar models have been constructed, each based on a single modification to the physics of a reference solar model. In addition, a model combining several of the improvements has been calculated to provide a "best" solar model. Improvements were made to the nuclear reaction rates, the equation of state, the opacities, and the treatment of the atmosphere. The impact on both the structure and the frequencies of the low-l p-modes of the model to these improvements are discussed. We find that the combined solar model, which is based on the best physics available to us (and does not contain any ad hoc assumptions), reproduces the observed oscillation spectrum (for low-l) within the errors associated with the uncertainties in the model physics (primarily opacities).

Subject headings: equation of state — Sun: interior — Sun: oscillations

1. INTRODUCTION

The enterprise of constructing solar models has a long and rich history; the introduction of new and improved physics has paralleled the development of successively more accurate models of the Sun. Solar models are crucial in our understanding of stars and stellar evolution, and continue to provide the best means of calibrating stellar models. In this paper we compare the properties of solar models constructed with the best available physics with the most sensitive test of the outer layers: namely, the frequencies of nonradial solar oscillations. We demonstrate that our "best" solar model reproduces the low-l p-mode oscillation frequencies within the errors associated with the physics of the model. We also discuss the impact of the individual improvements on the structure and the frequencies.

Lane (1869) first wrote down and solved the equations of a gas sphere in hydrostatic equilibrium to determine (without the aid of the Stefan-Boltzmann law, which had not yet been published) the Sun's surface temperature and density (he obtained $T_{\rm surface} = 30{,}000$ K and $\rho_{\rm surface} = 0.0004$ g cm^{-3}). Advances in atomic theory and the subsequent calculation of absorption coefficients for various atoms enabled Eddington (1926) to include a description of the transport of energy by radiation in his static solar and stellar models. The Sun's energy source was not incorporated in solar models until the discovery of thermonuclear reactions (Bethe 1939). The following decade was highlighted by the realization that the proton-proton chain, not the CN cycle, provides the principal source of nuclear energy in the Sun. Schwarzschild, Howard, & Härm (1957) calculated the first *evolutionary* models of the Sun, starting from the zero-age main sequence. The mixing-length theory of convection was first applied to the solar convection zone by Böhm-Vitense (1958). Needless to say, the introduction of computers resulted in a dramatic advance in the sophistication of the models, albeit, with relatively minor modifications to the actual structure predictions of the model. Computers have enabled more physics and more accurately modeled physics to be included in models of the Sun.

Models of other stars are constructed using the convective mixing-length parameter and the helium abundance (for disk population stars) determined from the solar model. The luminosity of stellar models strongly depends on the initial helium abundance and the radius of late-type stellar models strongly depends on the efficiency of convective energy transport. Helium can be seen only in stars with surface temperatures hot enough to ionize helium, where, unfortunately, non–LTE effects and gravitational settling of helium make abundance determinations difficult. Because helium is not visible in the optical spectrum of the Sun and because its abundance sensitively affects the luminosity of a solar model, it is used as an adjustable parameter of the solar model. The mixing-length theory characterizes the efficiency of convection in carrying the energy flux with a single parameter of order unity (α), which is the characteristic distance (in pressure scale heights) over which a convective element travels before merging with its surroundings. Because it sets the temperature gradients in the superadiabatic layers, it is responsible for fixing the location of a star's surface, i.e., its radius. Thus the mixing-length theory also provides, in the standard solar model, a convenient means of adjusting the solar radius to compensate for the other errors in the physics of the outer layers (Demarque & Percy 1964). The mixing-length parameter and the helium abundance are adjusted to produce a model which has the Sun's observed radius and luminosity; these values are then used in model calculations of other stars (Demarque & Larson 1964). It is within this context that the *standard solar model* first appeared in the literature.

Today, though, a standard solar model has come to mean many things to many authors (see, e.g., Sackmann, Boothroyd, & Fowler 1990). For example, it can represent a conservative model of the Sun based on well-established physics; it can represent an ever-improving model of the Sun, upgraded with each improvement made to current physics; or it can represent a solar model which best fits the observables of the Sun but relies on ad hoc adjustments to the physics. In this work we define our reference standard solar model to be a conservative model of the Sun based on well-established physics and calculate several improved solar models which upgrade the reference model by incorporating cutting-edge physics.

It is well known that the solar neutrino flux, as measured with the Davis chlorine detector (Davis 1978), is a factor of 2–3 times smaller than the predictions of solar models. As a consequence, over the past 20 years, hundreds of articles have been written describing various modifications to the standard solar

model which attempt to reconcile these discrepancies. In 1988, two independent studies of the solar model (Bahcall & Ulrich 1988; Turck-Chièze, Cahen, & Cassé 1988) focused on neutrino flux predictions and concluded that, once again, the standard physical assumptions of the standard solar model cannot be adjusted within the errors to account for the observed neutrino flux. This has led many to conclude that indeed the standard solar model is correct and it is the neutrino physics which is wrong (Bahcall & Pinsonneault 1991). In fact, the solar model and neutrino flux observations may ultimately establish the existence of resonant neutrino oscillations and the validity of nonstandard theories of electroweak interactions (Bahcall 1989; Mikheyev & Smirnov 1986; Wolfenstein 1978).

In recent years the very accurate determination of the frequencies of the Sun's p-modes (for example, Libbrecht, Woodard, & Kaufman 1990) and the persistent 1% discrepancy between these observations and model predictions has goaded solar modelers to adopt a more conservative approach, that of establishing the sensitivity of the model and its observables to variations or adjustments in the model parameters: age (Guenther 1989, 1991b); composition, opacities, and equation of state (Christensen-Dalsgaard, Däppen, & Lebreton 1988; Cox, Guzik, & Raby 1990; Guenther, Jaffe, & Demarque 1989; Guenther & Sarajedini 1988; Kim, Demarque, & Guenther 1991); envelope structure (Guenther 1991a; Ulrich & Rhodes 1977); and survey (Bahcall & Ulrich 1988; Christensen-Dalsgaard 1988; Ulrich & Rhodes 1983). The immediate goal is not to produce the ultimate fix to the standard solar model but to try to understand the importance of individual parameters to determining the accuracy with which one can expect the standard solar model to predict the frequencies of p-modes. Ulrich & Rhodes (1983) were able so show, in a definitive manner, that the standard solar model, and several nonstandard solar models, could not be easily tweaked within the known errors of the physics at that time, to reproduce the Sun's oscillation spectrum. In other words, they established, given what they believed to be reasonable estimates of the errors associated with the physics, that there is indeed a discrepancy between the p-mode spectrum predicted by the standard solar model and the Sun's p-mode spectrum.

In a key piece of research, Cox and his collaborators (Cox et al. 1990; Cox, Guzik, & Kidman 1989) demonstrated that solar models constructed with modified LAOL opacities (30% enhancement in convection zone) produce oscillation spectra in close agreement to the Sun's. The trick of enhancing the opacities to help fix the problem was first proposed by Christensen-Dalsgaard et al. (1985) and then elaborated on by Korzennik & Ulrich (1989). We show that similar ends can be obtained, without artificially modifying the calculated opacities, by using Iglesias & Rogers (1991) latest opacities (commonly referred to as the OPAL opacities) and either Cox's or Kurucz's low temperature "molecular" opacities.

In this paper we will continue our analysis of the sensitivity of the standard solar model to model assumptions and show that *a model of the Sun that makes no ad hoc assumptions but simply uses the best of today's physics can reproduce the solar p-mode oscillation spectrum within the errors of the physics used in the calculation of the standard solar model.* We present a conservative (reference) standard solar model and add commonly incorporated "improvements," one at a time, to determine the significance of their effect on the model, and to determine the approximate accuracy of today's standard solar models. We judge the "quality" of our models by comparing the frequencies of their p-mode spectra (of low-l) to the Sun's p-mode spectrum.

In § 2 we describe the physics and modeling procedure of our reference standard solar model and the augmented models. The augmented models include improvements to the atmosphere model, the nuclear reaction rates, the equation of state (MHD and Debye-Hückel), and opacities (Cox, Kurucz, and OPAL). In § 3 we describe the structural differences among the models and compare the low-l p-mode oscillation spectra of the models to the Sun's. In § 4 we summarize our results and comment on future directions.

2. THE SOLAR MODELS

2.1. *The Reference Standard Solar Model*

Our reference standard solar model (STD model) is constructed using the default physics and parameters of the Yale Rotating Stellar Evolution Code (Prather 1976; Pinsonneault 1988), in its nonrotating configuration, i.e., physics and parameters normally used for stellar evolutionary calculations. YREC (Yale Rotating Stellar Evolution Code) solves the conservation and transport equations of stellar structure using the Henyey relaxation method. The nuclear reaction network is solved separately for each shell in the model.

In the outer regions ($\log T < 5.5$), the equation-of-state routines determine particle densities by solving the Saha equation for the single ionization state of H and metals, and the single and double ionization states of He. In the inner regions the elements are assumed to be fully ionized. A small transition region is defined ($5.5 < \log T < 6.0$) where the interior formulation and exterior formulation are weighted with a ramp function and then averaged. Radiation pressure and electron degeneracy corrections are included but perturbations due to Coulomb interactions in the plasma (i.e., Debye-Hückel corrections) are ignored.

The opacity formulation is complicated by the fact that no single source of opacities covers the entire astrophysical regime. For $\log T > 4.0$, we use tables prepared using the LAOL tapes (Huebner et al. 1977). The tapes contain absorption coefficients for each of the 20 most abundant elements in the Sun as a function of temperature, electron degeneracy (itself a function of density and temperature), and photon frequency. With a modified version of LAOL tape combination software we construct Rosseland mean opacities in three-dimensional arrays of temperature, density, and hydrogen abundance for a specific mixture of heavy elements. For temperatures below 10,000 K, we interpolate the Cox & Stewart (1970) opacity tables to the appropriate X, Y, and Z (hydrogen, helium, and heavy element mass fraction) and integrate them into the LAOL opacity arrays. The opacity routines, within YREC, perform four-point Lagrangian interpolation of the tables. Note that the Cox & Stewart opacities are given for the obsolete Cox & Stewart mixture of heavy elements. A more extensive discussion of the opacity formulation is given in Guenther et al. (1989).

To produce our solar models we evolved a zero-age main-sequence model to the current age of the Sun in 50 equal time steps. Each model has approximately 1800 shells which are distributed equally among the interior (inner 95% by radius), the envelope (outer 5% by radius), and atmosphere. This spacetime mesh resolution is sufficient to produce models whose p-mode frequencies can be calculated to a numerical accuracy of ± 0.5 μHz with our pulsation code (Guenther &

Sarajedini 1988). The radius and luminosity of the models were matched to one part in 10^6 and one part in 10^5, respectively, by adjusting the mixing-length parameter and the helium mass fraction.

The age of the Sun can be inferred from the ages of the oldest meteorites. Although, the age is commonly quoted as being 4.6–4.7 Gyr, using the latest determinations of the ages of the oldest meteorites (Tilton 1988), modern theories of solar system formation, observations of T Tauri stars, and pre–main-sequence calculations, the best estimate of the Sun's age is 4.52 ± 0.4 Gyr. This number revises the 4.49 ± 0.03 Gyr age determined by Guenther (1989) (the difference is due to the use of the improved age estimates of the oldest meteorites by Tilton). Decimal prejudice, though, has lead us to adopt 4.5 Gyr for the solar age in all our solar models.

The mass of the Sun is 1.9891×10^{33} g with a relative uncertainty of $\pm 0.02\%$ (Cohen & Taylor 1986); the accuracy of the determination depends directly on the accuracy with which the Universal Gravitational Constant G is known. We adopt this mass for all our solar models.

The radius of the Sun, as determined by transit and eclipse measurements, is 6.96×10^{10} cm. As noted by Ulrich & Rhodes (1983), because the radius of the Sun for stellar structure calculations is defined at the optical depth of $\tau = \frac{2}{3}$ and eclipse and transit measurements are seeing only to a depth of $\tau = 0.001$ (at the limb), we adopt a solar radius of $R_\odot = 6.9598 \times 10^{10}$ cm at $\tau = \frac{2}{3}$ for all our solar models.

The luminosity has been determined from solar constant measurements from space on both the *Nimbus 7* and the *SMM* satellites (Hickey & Alton 1983). ERB-*Nimbus* measures 1371.6 ± 0.765 W m^{-2} and *SMM*/ACRIM measures 1367.7 ± 0.802 W m^{-2} which yield luminosities of 3.846×10^{33} ergs s^{-1} and 3.857×10^{33} ergs s^{-1}, respectively. As we cannot expertly base a preference, we merely take the average of the two and adopt the solar luminosity in all our models to be $L_\odot = 3.8515 \times 10^{33}$ ergs s^{-1}.

The mixture of heavy elements used in all the solar models, except the Ross-Aller mixture model and the MHD equation of state model, is that of Anders & Grevesse (1989) with $Z = 0.0188$.[1] The Ross-Aller mixture model and the MHD equation of state model use the Ross-Aller mixture (1976) with $Z = 0.02$. As noted in Guenther et al. (1989), the determination of the abundances of the elements is slowly converging to a specific mixture. Only the inert gases helium, neon, and argon remain poorly determined (note that neon is as abundant as nitrogen in the Sun).

Settling of helium and heavy elements by diffusion is not accounted for in any of the models presented here. This could cause differences between the current surface abundances and their initial values. The amount of diffusion is probably small, as is verified observationally by the close agreement between the meteoric and photospheric abundances (Anders & Grevesse 1989), which would be different if diffusion were important. Also, models by Cox et al. (1989) and by ourselves (presented at the Global Oscillation Network Group's annual meeting in Tucson, Arizona, 1991) show that the effects of helium diffusion on the frequencies of the low-l p-modes are very small.

Other physical characteristics of the STD model are summarized in Table 1. A summary of the internal structure of the model is listed in Table 3A.

All of the modified models, except the combined model, use the physics of the reference standard solar model with only one improvement incorporated at a time.

2.2. *Ross-Aller Mixture Model*

The Ross-Aller mixture model is similar to the STD model, except that the heavy element mixture is set to the popular Ross-Aller (1976) mixture with $Z = 0.02$. Opacities were calculated for this mixture using the LAOL tapes and software, described in the preceding section. Like all the other modified models, both the mixing-length parameter and the helium abundance were adjusted to produce a model with the proper radius and luminosity.

2.3. *MHD Equation of State Model*

The MHD equation-of-state tables (Mihalas, Däppen, & Hummer 1988; Mihalas et al. 1991; Hummer & Mihalas 1988) come from a new set of calculations, kindly provided to us by Däppen (1990), which offer a more realistic description of the atomic physics than modeled by our existing equation of state routines. The MHD equation of state formulation uses detailed internal partition functions for the specified mixture of atomic, ionic and molecular species. As provided for this test, the heavy element portion of the mixture, a Ross-Aller based mixture, consists of C, N, O with Ross-Aller abundance, and Fe adjusted to bring the total mass fraction of heavy elements to $Z = 0.02$.

The MHD equation of state model is similar to the Ross-Aller mixture model except that the standard equation-of-state routines in YREC are replaced with routines to look up values in the MHD equation-of-state tables. Note that for self-consistency we used the Ross-Aller mixture of heavy elements in the model calculation, including opacity tables based on the Ross-Aller mixture. The Ross-Aller model and the MHD equation of state model are described in detail in Kim et al. (1991).

2.4. *Debye-Hückel Correction*

The Debye-Hückel correction to the equation of state (Clayton 1968; Cox & Giuli 1968; Landau & Lifshitz 1959) attempts to take into account the Coulomb interactions of the plasma. The specific form implemented here from Clayton modifies the "perfect" pressure, P_p, i.e., ideal gas law pressure, by

$$P_g = P_p\left[1 - \frac{e^3}{3}\frac{(\pi N_0)^{1/2}}{k^{3/2}}\frac{\rho^{1/2}}{T^{3/2}}\mu\zeta^{3/2}\right],$$

where P_g is the gas pressure, N_0 is Avogadro's number, μ is the mean molecular weight, e is the charge of an electron, and k is Boltzmann's constant. The variable ζ is given by

$$\zeta \equiv \sum_i \left[(Z_i^2 + Z_i)\frac{X_i}{A_i}\right],$$

where Z_i, A_i, and X_i are the charge, atomic mass, and relative abundance by mass of element i. Assuming that Z is small compared to X and can be neglected, one obtains

$$P_g = P_p\left[1 - 0.044\frac{\rho^{1/2}(3 + X)^{3/2}}{T_6^{3/2}(5X + 3)}\right],$$

where T_6 is in units of 10^6 K. This form (note: formula published in Bahcall, Bahcall, & Shaviv 1968 is incorrect) is

[1] We have used solar photospheric abundances for all elements except iron, where we have used the meteoric abundance.

applicable in the regime of high temperature and low densities and assumes that the gas is fully ionized. This, therefore, is not the general form of the Debye-Hückel correction used in the detailed equation of state calculations of the MHD group. The general Debye-Hückel correction also takes into account partial ionization.

For temperatures above 10^6 K, YREC calls the Debye-Hückel correction routines after calling the standard equation of state routines to determine ρ, P, and T. Because YREC uses thermodynamic expressions to calculate quantities which depend on the derivatives of the pressure, temperature, and density, for example, to calculate the specific heat at constant pressure, these expressions were also modified to maintain thermodynamic consistency.[2] The model is then rerelaxed, and the process is iterated until a coveraged model is obtained.

2.5. *Cox Low-Temperature Opacities*

At low temperatures, our standard opacity tables use the Cox & Stewart (1970) opacities which do not include the effects of molecules. New tables which include the contribution of molecules, Ross-Aller 1 (Cox et al. 1989), have recently been made available to us (Cox 1990) for the Ross-Aller mixture (1976). These opacities are significantly larger than the Cox & Stewart (standard) tables, and, as is described in § 3, they have a profound effect on the p-mode oscillation spectrum.

The Cox low-temperature opacities model is similar to the STD model except that for temperatures and densities which fall within the range of the Cox low-T opacity tables ($\log T < 5$), they are used instead. To summarize: at temperatures above 10^5 K, the standard LAOL opacities for the Anders & Grevesse mixture are used, and at lower temperatures, the Cox low-T opacity tables for the Ross-Aller 1 mixture are used. We have not concerned ourselves with the inconsistency in the mixtures because (1) Kim et al. (1991) uses the Ross-Aller mixture throughout and obtains nearly identical results to those presented here, and (2) the Kurucz low-temperature opacity tables are included in our tests, and they are calculated for the Anders & Grevesse mixture, thereby providing a self-consistent test of low-temperature molecular opacities.

2.6. *Bahcall Nuclear Reaction Rates*

YREC's nuclear reaction rates are based on the proton-proton rates of Clayton (1968) and the CNO rates of Fowler, Caughlan, & Zimmerman (1975). To test how much the new rates, collected and published by Bahcall (1989), affect the p-mode frequencies, we implemented the new rates in YREC with a switch to turn them on, or off, where in the latter case the old rates are used. All of the models presented here, except the combined model and the Bahcall nuclear rates model, use the old nuclear reaction rates.

Note that comparisons made by Bahcall & Pinsonneault (1991) between our standard solar model (using the new rates) and Bahcall's solar model agree to 0.1%, with respect to pressure, temperature, density, luminosity, and composition, throughout most of the interior. The predicted neutrino fluxes of these models agree to 1%.

2.7. *Krishna Swamy Atmosphere Model*

The Krishna Swamy (1966) T-τ relation is a theoretically based empirical fit to the Sun's observed T-τ dependence in the lower atmosphere. The relation follows the drop in T from the surface of the photosphere, where $T_{\rm eff}$ is defined, at $\tau = 0.312156330$, to $\tau = 10^{-4}$. It does not model the temperature minimum at the base of the corona nor the temperature rise above. It is given by

$$T^4 = 0.75T_{\rm eff}^4(\tau + 1.39 - 0.815e^{-2.54\tau} - 0.025e^{-30\tau}) .$$

2.8. *Kurucz Low-Temperature Opacities Model*

The Kurucz (1991) low temperature opacities provide an improved opacity at lower temperatures by including the effects of molecules. Because they have been computed independently from the Cox molecular opacities, they also provide an independent check on the accuracy of the opacities. The Kurucz opacities, as provided to us in tabular form, are based on the Anders & Grevesse (1989) mixture, and are applicable at temperatures $\leq 10^4$ K.

2.9. *OPAL Opacities Model*

Recently, Iglesias & Rogers (1991) have made available to us their latest opacities calculated for the Anders & Grevesse mixture (hereafter referred to as the OPAL opacities). Unlike the LAOL opacities, which are provided for individual elements so that they can be combined by the user in an arbitrary mixture, the OPAL opacities are provided for a complete mixture only.[3]

The OPAL opacity model is similar to the STD model except that at temperatures above 10^6 K, the OPAL opacities are used instead of the LAOL opacities. Note that between 10^4 and 10^6 K, the LAOL opacities are used, and below 10^4 K, the Cox-Stewart opacities are used.

2.10. *Combined Model*

To demonstrate the additive effects of the individual modifications on the structure and p-mode frequencies and to present, in some sense, a "best" model, we have calculated a model which includes some of the above modifications. We did not include the MHD equation-of-state modification because it is based on the Ross-Aller mixture and not the Anders & Grevesse mixture used in the opacities. And for reasons discussed in § 3, we do not include the Debye-Hückel correction.

The combined model is based on the STD model with the following modifications: (1) OPAL opacities, (2) Kurucz low-temperature opacities, (3) Krishna Swamy atmosphere, and (4) Bahcall nuclear rates. Table 3B contains a summary of the details of this model's internal structure.

[2] Even though the structure and evolution of the Sun (and other stars) does not depend significantly on quantities derived from the derivatives of the fundamental variables (density, temperature, and pressure), the pulsation frequencies do. For example, the pulsation frequencies depend sensitively on the adiabatic exponent Γ_1. Therefore, it is especially important that thermodynamic consistency be maintained, in the fundamental variables and their derivatives, in stellar models destined to be used in pulsation calculations (M. Gabriel 1991, private communication).

[3] Recent reports made by C. A. Iglesias and A. Cox at the General Assembly of the IAU in Buenos Aires 1991 in a special session on opacities indicate that the OPAL opacities are to be preferred over the LAOL opacities because (1) they remove the disagreement between masses inferred from pulsation calculations and masses inferred from stellar evolution calculations, (2) it is believed that one set of lines associated with helium were incorrectly located in the LAOL opacity calculation (other errors associated with the iron lines were also noted), and (3) as reported in this paper, models based on the OPAL opacities better locate the base of the Sun's convection zone.

TABLE 1

MODEL CHARACTERISTICS

Model	Y	α	$\log(L/L_\odot)$	$\log(R/R_\odot)$	$\log(T_c)$	$\log(\rho_c)$	x_{conv}	$M_{conv}/M_\odot$	$\log(T_{conv})$
Standard model	0.2875	1.1949	−7.0E−6	8.2E−7	7.186	2.166	0.745	0.0153	6.284
Ross-Aller mixture	0.2843	1.2420	1.6E−7	−8.1E−7	7.190	2.166	0.738	0.0177	6.299
MHD equation of state	0.2736	1.2559	3.9E−7	−3.3E−7	7.188	2.159	0.734	0.0190	6.308
Debye-Hückel correction	0.2771	1.2225	−2.2E−6	−5.2E−8	7.185	2.160	0.740	0.0167	6.294
Cox low-temperature opacities	0.2876	2.0661	1.2E−5	6.0E−7	7.186	2.166	0.744	0.0153	6.285
Bahcall nuclear reaction rates	0.2843	1.1942	−1.1E−5	2.4E−7	7.189	2.181	0.744	0.0151	6.284
Krishna Swamy atmosphere	0.2875	1.4229	−2.7E−6	−1.2E−7	7.186	2.166	0.745	0.0155	6.284
Kurucz low-temperature opacities	0.2875	1.5588	1.4E−5	6.5E−8	7.186	2.166	0.745	0.0152	6.283
OPAL opacities	0.2918	1.2477	3.0E−6	1.3E−7	7.193	2.168	0.724	0.0211	6.331
Combined model	0.2892	1.8942	−1.4E−6	−3.5E−8	7.197	2.178	0.724	0.0210	6.330

3. RESULTS

3.1. *Structure Comparisons*

In Table 1 we list some of the characteristics of the models. In Table 2, discussed in § 3.2, we list the p-mode frequencies of the STD model and the combined model. And in Table 3 we list an abbreviated summary of the structure of the STD model and the combined model.

We see from Table 1 that there is very little variation in the helium mass fraction of the solar models, varying from $Y = 0.2736$ to $Y = 0.2918$. We are comfortable, therefore, in quoting the Sun's interior helium abundance to be $Y = 0.28 \pm 0.01$.

The mixing-length parameter, as expected, depends primarily on the details of the surface layers. The Krishna Swamy model, the Cox opacity model, and the Kurucz opacity model

TABLE 2A

STANDARD MODEL: p-MODE FREQUENCIES AND SPACINGS

	$l = 0$			$l = 1$			$l = 2$		$l = 3$	
n	ν	$\Delta\nu$	$\delta\nu$	ν	$\Delta\nu$	$\delta\nu$	ν	$\Delta\nu$	ν	$\Delta\nu$
1	402.423	0.000	0.000	448.229	0.000	0.000	379.326	0.000	414.395	0.000
2	533.610	131.187	0.000	0.000	0.000	0.000	513.470	134.144	563.226	148.832
3	676.282	142.672	0.000	595.069	0.000	31.842	660.830	147.360	714.639	151.413
4	820.660	144.377	0.000	743.612	148.543	28.972	807.630	146.800	860.862	146.223
5	0.000	0.000	0.000	887.493	143.881	26.630	953.177	145.547	1007.755	146.893
6	966.338	0.000	13.161	1032.608	145.115	24.853	1097.017	143.840	1152.198	144.443
7	1110.182	143.843	13.165	1176.500	143.892	24.301	1241.403	144.386	1296.747	144.549
8	1254.726	144.544	13.323	1319.908	143.408	23.161	1383.587	142.184	1439.159	142.411
9	1396.872	142.147	13.285	1461.714	141.806	22.556	1524.139	140.553	1578.550	139.391
10	1536.990	140.118	12.851	1600.005	138.291	21.455	1661.207	137.068	1715.711	137.161
11	1673.810	136.820	12.602	1736.605	136.600	20.895	1796.982	135.774	1851.678	135.967
12	1809.197	135.387	12.216	1872.334	135.729	20.656	1933.441	136.459	1988.858	137.180
13	1945.463	136.266	12.022	2009.068	136.734	20.211	2070.123	136.683	2125.957	137.099
14	2081.790	136.327	11.666	2145.745	136.677	19.789	2206.744	136.621	2262.268	136.311
15	2217.943	136.154	11.199	2281.295	135.550	19.027	2341.941	135.197	2397.703	135.435
16	2352.759	134.816	10.818	2416.187	134.893	18.485	2476.705	134.764	2532.718	135.015
17	2487.124	134.364	10.419	2550.774	134.587	18.057	2611.986	135.281	2668.779	136.061
18	2622.163	135.039	10.177	2686.398	135.623	17.619	2747.983	135.997	2805.493	136.715
19	2757.871	135.708	9.888	2822.747	136.350	17.254	2884.840	136.857	2942.699	137.205
20	2894.414	136.543	9.574	2959.427	136.679	16.728	3021.707	136.867	3080.079	137.381
21	3030.984	136.570	9.277	3096.369	136.943	16.290	3158.836	137.128	3217.451	137.372
22	3167.785	136.801	8.949	3233.278	136.909	15.827	3296.170	137.335	3355.320	137.869
23	3304.871	137.086	8.701	3370.704	137.427	15.384	3433.833	137.663	3493.431	138.111
24	3442.266	137.395	8.433	3508.423	137.719	14.992	3572.017	138.184	3631.987	138.556
25	3580.213	137.948	8.196	3646.522	138.099	14.536	3710.322	138.305	3770.734	138.747
26	3718.288	138.075	7.966	3784.876	138.353	14.142	3848.929	138.607	3909.584	138.851
27	3856.661	138.373	7.733	3923.302	138.427	13.718	3987.588	138.660	4048.674	139.090
28	3995.122	138.461	7.534	4062.018	138.715	13.343	4126.444	138.855	4187.784	139.109
29	4133.761	138.639	7.317	4200.767	138.749	12.983	4265.483	139.039	4327.124	139.340
30	4272.616	138.856	7.133	4339.736	138.969	12.612	4404.544	139.061	4466.444	139.320
31	4411.488	138.872	6.944	4478.723	138.987	12.279	4543.724	139.180	4605.775	139.331
32	4550.492	139.004	6.767	4617.695	138.972	11.919	4682.756	139.031	4745.030	139.255
33	4689.359	138.867	6.603	4756.629	138.935	11.599	4821.745	138.989	4884.067	139.037
34	4828.180	138.822	6.435	4895.333	138.703	11.265	4960.476	138.731	5022.893	138.825
35	4966.763	138.582	6.287	5033.833	138.500	10.940	5098.803	138.328	5161.103	138.210
36	5104.926	138.163	6.122	5171.716	137.883	10.613	5236.443	137.640	5298.397	137.294
37	5242.402	137.476	5.958	5308.639	136.923	10.242	5372.665	136.221	5433.815	135.418
38	5378.427	136.025	5.762	5443.631	134.992	9.817	5506.300	133.635	5565.570	131.755
39	5511.801	133.374	5.501	5574.780	131.149	9.210	5634.600	128.300	5690.386	124.816
40	5639.719	127.918	5.119	5698.778	123.997	8.392	5754.292	119.692	5806.572	116.186
41	5758.970	119.251	4.678	5814.400	115.622	7.828	5868.768	114.477	5922.680	116.108

TABLE 2B

COMBINED MODEL: *p*-MODE FREQUENCIES AND SPACINGS

	$l = 0$			$l = 1$			$l = 2$		$l = 3$	
n	ν	$\Delta\nu$	$\delta\nu$	ν	$\Delta\nu$	$\delta\nu$	ν	$\Delta\nu$	ν	$\Delta\nu$
1.....	404.202	0.000	0.000	448.609	0.000	0.000	382.616	0.000	416.105	0.000
2.....	535.340	131.138	0.000	0.000	0.000	0.000	514.656	132.039	564.890	148.785
3.....	679.252	143.912	0.000	596.748	0.000	31.858	663.761	149.105	717.714	152.824
4.....	823.045	143.794	0.000	745.705	148.957	27.991	810.076	146.315	864.535	146.821
5.....	0.000	0.000	0.000	891.016	145.311	26.481	956.743	146.668	1011.582	147.048
6.....	969.300	0.000	12.557	1036.027	145.011	24.444	1101.048	144.304	1157.112	145.530
7.....	1113.756	144.455	12.708	1181.046	145.020	23.934	1245.873	144.826	1301.506	144.394
8.....	1258.525	144.770	12.652	1324.359	143.313	22.853	1388.766	142.892	1444.660	143.154
9.....	1401.579	143.054	12.813	1466.631	142.272	21.971	1529.084	140.319	1583.999	139.339
10.....	1541.528	139.950	12.444	1605.214	138.582	21.215	1666.896	137.812	1721.371	137.372
11.....	1679.126	137.598	12.230	1741.794	136.580	20.422	1802.807	135.911	1858.021	136.649
12.....	1814.920	135.794	12.114	1878.289	136.496	20.269	1939.565	136.759	1995.061	137.041
13.....	1951.444	136.524	11.879	2014.928	136.638	19.866	2076.454	136.889	2132.330	137.269
14.....	2088.119	136.675	11.665	2151.640	136.712	19.309	2212.413	135.959	2268.062	135.731
15.....	2223.620	135.501	11.207	2286.860	135.220	18.798	2347.380	134.967	2402.828	134.767
16.....	2358.172	134.552	10.792	2421.023	134.163	18.195	2481.473	134.093	2537.565	134.736
17.....	2491.975	133.803	10.501	2555.447	134.424	17.882	2616.231	134.758	2672.814	135.250
18.....	2626.406	134.431	10.175	2690.362	134.915	17.548	2751.818	135.587	2809.001	136.187
19.....	2761.731	135.325	9.912	2826.098	135.736	17.096	2887.666	135.847	2945.286	136.284
20.....	2897.246	135.515	9.580	2961.988	135.891	16.703	3023.824	136.158	3081.632	136.346
21.....	3033.064	135.818	9.240	3097.844	135.856	16.213	3159.956	136.132	3218.320	136.688
22.....	3168.923	135.859	8.968	3234.127	136.283	15.807	3296.479	136.523	3355.252	136.932
23.....	3305.149	136.225	8.670	3370.678	136.551	15.426	3433.540	137.061	3492.758	137.505
24.....	3441.961	136.812	8.421	3507.743	137.065	14.986	3570.828	137.288	3630.517	137.759
25.....	3578.996	137.035	8.168	3645.123	137.380	14.607	3708.509	137.681	3768.442	137.925
26.....	3716.421	137.425	7.911	3782.620	137.497	14.178	3846.298	137.789	3906.663	138.221
27.....	3853.996	137.576	7.698	3920.446	137.826	13.783	3984.288	137.990	4044.962	138.299
28.....	3991.760	137.764	7.472	4058.379	137.932	13.417	4122.560	138.271	4183.541	138.579
29.....	4129.837	138.077	7.278	4196.566	138.187	13.024	4260.896	138.336	4322.227	138.686
30.....	4267.985	138.148	7.089	4334.908	138.342	12.681	4399.426	138.530	4460.923	138.696
31.....	4406.326	138.341	6.900	4473.239	138.331	12.316	4537.937	138.511	4599.720	138.797
32.....	4544.677	138.351	6.740	4611.695	138.456	11.975	4676.456	138.519	4738.414	138.694
33.....	4683.028	138.351	6.571	4750.069	138.374	11.655	4815.003	138.546	4877.102	138.688
34.....	4821.427	138.399	6.424	4888.421	138.352	11.319	4953.364	138.361	5015.622	138.521
35.....	4959.645	138.218	6.281	5026.639	138.218	11.017	5091.588	138.225	5153.824	138.202
36.....	5097.725	138.079	6.136	5164.520	137.882	10.696	5229.396	137.808	5291.600	137.776
37.....	5235.400	137.675	6.004	5301.978	137.458	10.378	5366.559	137.163	5428.500	136.900
38.....	5372.413	137.013	5.855	5438.555	136.577	10.055	5502.720	136.161	5564.108	135.608
39.....	5508.421	136.007	5.700	5573.788	135.234	9.681	5637.050	134.330	5697.433	133.326
40.....	5642.566	134.145	5.515	5706.689	132.900	9.255	5768.388	131.337	5826.901	129.468
41.....	5773.657	131.092	5.270	5835.627	128.938	8.725	5894.991	126.604	5951.168	124.266

all require larger mixing-length parameters. Equivalently, models whose modifications do not affect the surface layers have little effect on the mixing-length parameter. Although the relative changes are interesting, the actual value of the mixing-length parameter should not be given any significance because it depends on the specific mixing length formalism used in the stellar evolution code.

The interior temperature and densities of the different models are remarkably similar. The larges changes to the central temperature were effected by changing the composition (compare the standard model to the Ross-Aller model) and by changing the high temperature opacities (compare the standard model to the OPAL model). The largest changes to the central density were effected by changing the equation of state. With respect to the fundamental variables, pressure, temperature, and density, the Debye-Hückel model is very similar to the MHD model.

One true success of helioseismology is the determination of the physical location of the base of the surface convection zone. Christensen-Dalsgaard, Gough, & Thompson (1991) have inverted the Sun's *p*-mode oscillation frequencies to determine its radius fraction location to be $x_{\rm conv} = 0.713 \pm 0.003$. Unfortunately, our standard solar model positions the base of the convection zone significantly higher up at $x_{\rm conv} = 0.745 \pm 0.005$ (error based on shell resolution at this depth). Enhancing the opacities near the base of the convection, as the OPAL opacities do, significantly alleviates this discrepancy. The base of the convection zone in the OPAL model is $x_{\rm conv} = 0.724 \pm 0.005$. The MHD equation of state (compare to Ross-Aller model) and the Debye-Hückel correction (compare to standard model) both deepen the base of the convection zone. Our results suggest that a model incorporating both the MHD equation of state and the OPAL opacities will further improve the near agreement.

The temperature at the base of the convection zone is also greater for the models with deeper convection zones, thus raising the question, "what about lithium?" One *cannot* simply deepen the convection zone to resolve the "lithium problem." Because lithium is a relatively fragile element in stellar interiors, its depeletion is a sensitive indicator of both the depth of the surface convection zone as a function of time and the nature of mixing at and below the base of the surface

TABLE 3A

SUMMARY OF REFERENCE STANDARD MODEL

Shell	Radius Frac	Mass Frac	Temperature	Density	Pressure	Sound Speed	Brunt V Sq
	Mean Mol Wt	Luminosity	Nuc Rate	Opacity	Temp Grad	Ad Temp Grad	Gamma 1
1	6.59279E-03	2.97851E-05	1.53362E+07	1.46442E+02	2.25772E+17	5.06369E+07	1.29244E-07
	8.44467E-01	9.60367E+29	1.62049E+01	1.18874E+00	3.10057E-01	3.98342E-01	1.66315E+00
21	2.26567E-02	1.18576E-03	1.51942E+07	1.41528E+02	2.19119E+17	5.07446E+07	1.38195E-06
	8.32887E-01	3.76902E+31	1.57226E+01	1.20031E+00	3.10890E-01	3.98361E-01	1.66319E+00
41	6.25625E-02	2.18814E-02	1.42894E+07	1.14376E+02	1.79770E+17	5.11322E+07	6.30116E-06
	7.70284E-01	6.10790E+32	1.25188E+01	1.29775E+00	3.09587E-01	3.98471E-01	1.66343E+00
61	9.03622E-02	5.76113E-02	1.33688E+07	9.27050E+01	1.44932E+17	5.09994E+07	7.92449E-06
	7.23463E-01	1.38084E+33	9.37555E+00	1.42807E+00	3.07819E-01	3.98574E-01	1.66367E+00
81	1.16439E-01	1.06966E-01	1.24198E+07	7.46674E+01	1.13816E+17	5.03615E+07	8.02882E-06
	6.88401E-01	2.15162E+33	6.51958E+00	1.57833E+00	3.01008E-01	3.98673E-01	1.66389E+00
101	1.48492E-01	1.84555E-01	1.12474E+07	5.64466E+01	8.12809E+16	4.89519E+07	7.43215E-06
	6.58875E-01	2.92272E+33	3.73445E+00	1.80989E+00	2.88539E-01	3.98783E-01	1.66413E+00
121	1.87861E-01	2.96050E-01	9.87881E+06	3.93712E+01	5.12591E+16	4.65505E+07	6.67498E-06
	6.38813E-01	3.48764E+33	1.61449E+00	2.18116E+00	2.74113E-01	3.98896E-01	1.66439E+00
141	2.24081E-01	4.04062E-01	8.73438E+06	2.77295E+01	3.22979E+16	4.40323E+07	6.47782E-06
	6.30218E-01	3.71898E+33	6.64190E-01	2.55884E+00	2.59052E-01	3.98981E-01	1.66460E+00
161	2.58253E-01	5.02593E-01	7.77668E+06	1.95477E+01	2.03557E+16	4.16361E+07	6.53547E-06
	6.26616E-01	3.80528E+33	2.68752E-01	2.92226E+00	2.44073E-01	3.99038E-01	1.66475E+00
181	2.91183E-01	5.89337E-01	6.97318E+06	1.37295E+01	1.28312E+16	3.94453E+07	6.64578E-06
	6.25124E-01	3.83591E+33	1.08349E-01	3.26144E+00	2.28339E-01	3.99068E-01	1.66486E+00
201	3.23493E-01	6.63940E-01	6.30103E+06	9.58143E+00	8.08899E+15	3.74911E+07	6.68388E-06
	6.24508E-01	3.84648E+33	4.39944E-02	3.59010E+00	2.11548E-01	3.99072E-01	1.66492E+00
221	3.55688E-01	7.27101E-01	5.72663E+06	6.65147E+00	5.09978E+15	3.57287E+07	6.29191E-06
	6.24253E-01	3.85005E+33	1.79460E-02	4.08363E+00	2.03233E-01	3.99056E-01	1.66494E+00
241	3.88111E-01	7.79975E-01	5.22214E+06	4.60212E+00	3.21538E+15	3.41064E+07	5.79443E-06
	6.24145E-01	3.85121E+33	7.29397E-03	4.65452E+00	1.96947E-01	3.99023E-01	1.66493E+00
261	4.21011E-01	8.23851E-01	4.77405E+06	3.17620E+00	2.02736E+15	3.25991E+07	5.22855E-06
	6.24100E-01	3.85155E+33	2.94674E-03	5.31783E+00	1.92321E-01	3.98973E-01	1.66490E+00
281	4.54574E-01	8.59993E-01	4.37275E+06	2.18766E+00	1.27833E+15	3.11901E+07	4.66685E-06
	6.24081E-01	3.85162E+33	1.18089E-03	6.08121E+00	1.88749E-01	3.98905E-01	1.66483E+00
301	4.88938E-01	8.89572E-01	4.00870E+06	1.50529E+00	8.06058E+14	2.98569E+07	4.06728E-06
	6.24074E-01	3.85161E+33	4.67161E-04	7.05749E+00	1.89052E-01	3.98821E-01	1.66473E+00
321	5.24153E-01	9.13633E-01	3.66983E+06	1.03714E+00	5.08273E+14	2.85619E+07	3.44934E-06
	6.24069E-01	3.85158E+33	1.80130E-04	8.33605E+00	1.95192E-01	3.98731E-01	1.66463E+00
341	5.60156E-01	9.33081E-01	3.35039E+06	7.16477E-01	3.20501E+14	2.72872E+07	2.96007E-06
	6.24069E-01	3.85154E+33	6.70702E-05	9.58331E+00	1.99434E-01	3.98641E-01	1.66453E+00
361	5.96846E-01	9.48688E-01	3.05216E+06	4.96007E-01	2.02098E+14	2.60417E+07	2.52975E-06
	6.24068E-01	3.85152E+33	0.00000E+00	1.09607E+01	2.05402E-01	3.98549E-01	1.66442E+00
381	6.34062E-01	9.61115E-01	2.77054E+06	3.44585E-01	1.27434E+14	2.48093E+07	2.13191E-06
	6.24068E-01	3.85150E+33	0.00000E+00	1.25323E+01	2.15295E-01	3.98465E-01	1.66433E+00

TABLE 3A—*Continued*

Shell	Radius Frac Mean Mol Wt	Mass Frac Luminosity	Temperature Nuc Rate	Density Opacity	Pressure Temp Grad	Sound Speed Ad Temp Grad	Brunt V Sq Gamma 1
401	6.71531E-01	9.70925E-01	2.49952E+06	2.40853E-01	8.03535E+13	2.35634E+07	1.73071E-06
	6.24068E-01	3.85148E+33	0.00000E+00	1.43997E+01	2.33075E-01	3.98409E-01	1.66427E+00
421	7.08787E-01	9.78588E-01	2.22779E+06	1.70405E-01	5.06653E+13	2.22449E+07	1.21843E-06
	6.24068E-01	3.85147E+33	0.00000E+00	1.69323E+01	2.71692E-01	3.98422E-01	1.66431E+00
441	7.44901E-01	9.84497E-01	1.92278E+06	1.24514E-01	3.19461E+13	2.06659E+07	5.84363E-08
	6.24068E-01	3.85146E+33	0.00000E+00	2.18262E+01	3.95556E-01	3.98612E-01	1.66460E+00
461	7.77455E-01	9.88880E-01	1.60659E+06	9.49891E-02	2.03581E+13	1.88906E+07	-6.07092E-12
	6.24068E-01	3.85145E+33	0.00000E+00	2.95143E+01	3.98930E-01	3.98929E-01	1.66506E+00
481	8.07434E-01	9.92209E-01	1.33662E+06	7.20190E-02	1.28389E+13	1.72307E+07	-8.76175E-12
	6.24068E-01	3.85144E+33	0.00000E+00	3.79198E+01	3.99180E-01	3.99179E-01	1.66543E+00
501	8.34105E-01	9.94620E-01	1.11195E+06	5.46092E-02	8.09764E+12	1.57161E+07	-1.28669E-11
	6.24068E-01	3.85144E+33	0.00000E+00	4.94738E+01	3.99371E-01	3.99370E-01	1.66571E+00
521	8.57616E-01	9.96331E-01	9.24996E+05	4.14128E-02	5.10760E+12	1.43340E+07	-5.32387E-09
	6.23808E-01	3.85144E+33	0.00000E+00	6.59040E+01	3.99516E-01	3.99514E-01	1.66592E+00
541	8.78165E-01	9.97527E-01	7.69453E+05	3.14349E-02	3.22181E+12	1.30674E+07	-4.61349E-08
	6.24382E-01	3.85143E+33	0.00000E+00	8.96268E+01	3.99566E-01	3.99564E-01	1.66608E+00
561	8.95972E-01	9.98349E-01	6.40093E+05	2.39014E-02	2.03237E+12	1.19026E+07	-9.65950E-08
	6.26023E-01	3.85143E+33	0.00000E+00	1.25181E+02	3.99388E-01	3.99384E-01	1.66611E+00
581	9.11281E-01	9.98907E-01	5.32574E+05	1.81923E-02	1.28210E+12	1.08350E+07	-1.23613E-07
	6.28421E-01	3.85143E+33	0.00000E+00	1.81058E+02	3.98847E-01	3.98842E-01	1.66582E+00
601	9.24365E-01	9.99282E-01	4.43277E+05	1.38420E-02	8.08827E+11	9.86350E+06	-1.03858E-07
	6.30826E-01	3.85143E+33	0.00000E+00	2.82153E+02	3.97851E-01	3.97844E-01	1.66497E+00
621	9.35506E-01	9.99531E-01	3.69168E+05	1.05145E-02	5.10269E+11	8.98455E+06	-4.03250E-08
	6.32544E-01	3.85143E+33	0.00000E+00	5.04975E+02	3.96355E-01	3.96345E-01	1.66334E+00
641	9.44973E-01	9.99695E-01	3.07706E+05	7.97181E-03	3.21923E+11	8.18884E+06	-3.01789E-10
	6.33589E-01	3.85143E+33	0.00000E+00	9.17142E+02	3.94172E-01	3.94158E-01	1.66054E+00
661	9.53106E-01	9.99804E-01	2.56160E+05	6.01517E-03	2.01795E+11	7.45127E+06	-5.31966E-10
	6.34906E-01	3.85143E+33	0.00000E+00	1.63396E+03	3.90314E-01	3.90295E-01	1.65500E+00
681	9.59883E-01	9.99874E-01	2.14320E+05	4.55051E-03	1.27324E+11	6.78316E+06	-8.70517E-10
	6.36895E-01	3.85143E+33	0.00000E+00	2.76241E+03	3.83549E-01	3.83522E-01	1.64442E+00
701	9.65615E-01	9.99919E-01	1.80046E+05	3.43406E-03	8.03361E+10	6.16725E+06	-1.43950E-09
	6.39930E-01	3.85143E+33	0.00000E+00	4.43861E+03	3.72463E-01	3.72426E-01	1.62585E+00
721	9.70469E-01	9.99948E-01	1.52179E+05	2.58121E-03	5.06886E+10	5.60385E+06	-2.41228E-09
	6.44342E-01	3.85143E+33	0.00000E+00	6.73862E+03	3.57370E-01	3.57319E-01	1.59914E+00
741	9.74591E-01	9.99966E-01	1.29545E+05	1.93037E-03	3.19823E+10	5.10251E+06	-4.03469E-09
	6.50130E-01	3.85143E+33	0.00000E+00	1.05191E+04	3.42563E-01	3.42493E-01	1.57144E+00
761	9.78104E-01	9.99978E-01	1.10876E+05	1.43751E-03	2.01795E+10	4.67282E+06	-6.67950E-09
	6.56733E-01	3.85143E+33	0.00000E+00	1.67495E+04	3.35003E-01	3.34906E-01	1.55547E+00
781	9.81103E-01	9.99986E-01	9.49835E+04	1.06935E-03	1.27324E+10	4.31055E+06	-1.10195E-08
	6.63287E-01	3.85143E+33	0.00000E+00	2.63584E+04	3.38713E-01	3.38572E-01	1.56054E+00

TABLE 3A—*Continued*

Shell	Radius Frac	Mass Frac	Temperature	Density	Pressure	Sound Speed	Brunt V Sq
	Mean Mol Wt	Luminosity	Nuc Rate	Opacity	Temp Grad	Ad Temp Grad	Gamma 1
801	9.83658E-01	9.99991E-01	8.10910E+04	7.97557E-04	8.03361E+09	3.98896E+06	-1.82600E-08
	6.69371E-01	3.85143E+33	0.00000E+00	3.70233E+04	3.47727E-01	3.47520E-01	1.57968E+00
821	9.85827E-01	9.99994E-01	6.90634E+04	5.96497E-04	5.06886E+09	3.66990E+06	-3.05247E-08
	6.75752E-01	3.85143E+33	0.00000E+00	4.66387E+04	3.46744E-01	3.46454E-01	1.58491E+00
841	9.87665E-01	9.99996E-01	5.90808E+04	4.45295E-04	3.19823E+09	3.34606E+06	-5.00334E-08
	6.83951E-01	3.85143E+33	0.00000E+00	5.46285E+04	3.28710E-01	3.28329E-01	1.55885E+00
861	9.89229E-01	9.99997E-01	5.11054E+04	3.30045E-04	2.01795E+09	3.04068E+06	-7.92287E-08
	6.94976E-01	3.85143E+33	0.00000E+00	6.38410E+04	3.00199E-01	2.99720E-01	1.51219E+00
881	9.90570E-01	9.99998E-01	4.48136E+04	2.42230E-04	1.27324E+09	2.77320E+06	-1.22461E-07
	7.08871E-01	3.85143E+33	0.00000E+00	7.49210E+04	2.70891E-01	2.70300E-01	1.46312E+00
901	9.91732E-01	9.99999E-01	3.97891E+04	1.76077E-04	8.03361E+08	2.54755E+06	-1.87590E-07
	7.25101E-01	3.85143E+33	0.00000E+00	8.46051E+04	2.46590E-01	2.45854E-01	1.42246E+00
921	9.92746E-01	9.99999E-01	3.56762E+04	1.26985E-04	5.06886E+08	2.35721E+06	-2.87331E-07
	7.43128E-01	3.85143E+33	0.00000E+00	8.96821E+04	2.28118E-01	2.27187E-01	1.39200E+00
941	9.93638E-01	9.99999E-01	3.22298E+04	9.10248E-05	3.19823E+08	2.19287E+06	-4.40212E-07
	7.62688E-01	3.85143E+33	0.00000E+00	8.31830E+04	2.13537E-01	2.12345E-01	1.36859E+00
961	9.94427E-01	9.99999E-01	2.92993E+04	6.49198E-05	2.01795E+08	2.04705E+06	-6.71923E-07
	7.83726E-01	3.85143E+33	0.00000E+00	6.64388E+04	2.00603E-01	1.99074E-01	1.34810E+00
981	9.95127E-01	9.99999E-01	2.67904E+04	4.60835E-05	1.27324E+08	1.91561E+06	-1.01872E-06
	8.06224E-01	3.85143E+33	0.00000E+00	4.99525E+04	1.88262E-01	1.86306E-01	1.32816E+00
1001	9.95752E-01	9.99999E-01	2.46323E+04	3.25604E-05	8.03361E+07	1.79683E+06	-1.53435E-06
	8.30094E-01	3.85143E+33	0.00000E+00	3.65808E+04	1.76640E-01	1.74137E-01	1.30857E+00
1021	9.96312E-01	9.99999E-01	2.27637E+04	2.29033E-05	5.06886E+07	1.68966E+06	-2.30008E-06
	8.55215E-01	3.85143E+33	0.00000E+00	2.63576E+04	1.66201E-01	1.62983E-01	1.29000E+00
1041	9.96815E-01	9.99999E-01	2.11312E+04	1.60461E-05	3.19823E+07	1.59287E+06	-3.43856E-06
	8.81509E-01	3.85143E+33	0.00000E+00	1.84638E+04	1.57254E-01	1.53077E-01	1.27298E+00
1061	9.97270E-01	9.99999E-01	1.96894E+04	1.12044E-05	2.01795E+07	1.50503E+06	-5.13492E-06
	9.08992E-01	3.85143E+33	0.00000E+00	1.26542E+04	1.49924E-01	1.44442E-01	1.25768E+00
1081	9.97682E-01	9.99999E-01	1.84010E+04	7.80424E-06	1.27324E+07	1.42466E+06	-7.67077E-06
	9.37798E-01	3.85143E+33	0.00000E+00	8.70829E+03	1.44285E-01	1.36998E-01	1.24406E+00
1101	9.98056E-01	9.99999E-01	1.72344E+04	5.42790E-06	8.03361E+06	1.35035E+06	-1.14807E-05
	9.68208E-01	3.85143E+33	0.00000E+00	6.07578E+03	1.40478E-01	1.30652E-01	1.23201E+00
1121	9.98395E-01	9.99999E-01	1.61625E+04	3.77437E-06	5.06886E+06	1.28075E+06	-1.72509E-05
	1.00067E+00	3.85143E+33	0.00000E+00	4.27092E+03	1.38819E-01	1.25355E-01	1.22142E+00
1141	9.98703E-01	9.99999E-01	1.51595E+04	2.62831E-06	3.19823E+06	1.21455E+06	-2.61008E-05
	1.03587E+00	3.85143E+33	0.00000E+00	2.98850E+03	1.39966E-01	1.21148E-01	1.21228E+00
1161	9.98982E-01	9.99999E-01	1.41987E+04	1.83695E-06	2.01795E+06	1.15042E+06	-3.99531E-05
	1.07471E+00	3.85143E+33	0.00000E+00	2.00974E+03	1.45253E-01	1.18248E-01	1.20476E+00
1181	9.99233E-01	9.99999E-01	1.32472E+04	1.29275E-06	1.27324E+06	1.08689E+06	-6.23892E-05
	1.11839E+00	3.85143E+33	0.00000E+00	1.22862E+03	1.57541E-01	1.17260E-01	1.19944E+00

TABLE 3A—*Continued*

Shell	Radius Frac	Mass Frac	Temperature	Density	Pressure	Sound Speed	Brunt V Sq
	Mean Mol Wt	Luminosity	Nuc Rate	Opacity	Temp Grad	Ad Temp Grad	Gamma 1
1201	9.99457E-01	9.99999E-01	1.22553E+04	9.20911E-07	8.03361E+05	1.02235E+06	-1.01068E-04
	1.16815E+00	3.85143E+33	0.00000E+00	6.64830E+02	1.83818E-01	1.19857E-01	1.19815E+00
1221	9.99653E-01	1.00000E+00	1.11261E+04	6.70827E-07	5.06886E+05	9.55180E+05	-1.77152E-04
	1.22437E+00	3.85143E+33	0.00000E+00	2.80056E+02	2.45575E-01	1.31617E-01	1.20745E+00
1241	9.99820E-01	1.00000E+00	9.59173E+03	5.14107E-07	3.19823E+05	8.86933E+05	-3.90276E-04
	1.28205E+00	3.85143E+33	0.00000E+00	6.11592E+01	4.43093E-01	1.80196E-01	1.26451E+00
1261	9.99948E-01	1.00000E+00	6.66630E+03	4.78023E-07	2.01795E+05	8.23619E+05	-1.10080E-03
	1.31301E+00	3.85143E+33	0.00000E+00	1.34541E+00	9.92572E-01	3.75309E-01	1.60690E+00
1281	1.00001E+00	1.00000E+00	5.65969E+03	4.09416E-07	1.46666E+05	7.70572E+05	2.13061E-04
	1.31363E+00	3.85143E+33	0.00000E+00	2.69684E-01	2.94277E-01	3.96370E-01	1.65753E+00
1301	1.00004E+00	1.00000E+00	5.40473E+03	3.53976E-07	1.21090E+05	7.53952E+05	4.42588E-04
	1.31366E+00	3.85143E+33	0.00000E+00	1.80790E-01	1.95852E-01	3.98018E-01	1.66170E+00
1321	1.00008E+00	1.00000E+00	5.22317E+03	2.95953E-07	9.78395E+04	7.41494E+05	6.09300E-04
	1.31367E+00	3.85143E+33	0.00000E+00	1.29405E-01	1.29859E-01	3.98572E-01	1.66312E+00
1341	1.00012E+00	1.00000E+00	5.09808E+03	2.41105E-07	7.77978E+04	7.32662E+05	7.29226E-04
	1.31368E+00	3.85143E+33	0.00000E+00	9.66965E-02	8.50149E-02	3.98751E-01	1.66359E+00
1361	1.00016E+00	1.00000E+00	5.01415E+03	1.92615E-07	6.11284E+04	7.26640E+05	8.12902E-04
	1.31368E+00	3.85143E+33	0.00000E+00	7.43968E-02	5.49227E-02	3.98807E-01	1.66374E+00
1381	1.00020E+00	1.00000E+00	4.95894E+03	1.51665E-07	4.76031E+04	7.22639E+05	8.69512E-04
	1.31368E+00	3.85143E+33	0.00000E+00	5.84743E-02	3.51388E-02	3.98819E-01	1.66377E+00
1401	1.00025E+00	1.00000E+00	4.92314E+03	1.18206E-07	3.68338E+04	7.20026E+05	9.06742E-04
	1.31368E+00	3.85143E+33	0.00000E+00	4.66911E-02	2.23489E-02	3.98810E-01	1.66376E+00
1421	1.00029E+00	1.00000E+00	4.90014E+03	9.14680E-08	2.83691E+04	7.18337E+05	9.30851E-04
	1.31368E+00	3.85143E+33	0.00000E+00	3.76722E-02	1.41506E-02	3.98788E-01	1.66371E+00
1441	1.00033E+00	1.00000E+00	4.88546E+03	7.04133E-08	2.17738E+04	7.17249E+05	9.46233E-04
	1.31368E+00	3.85143E+33	0.00000E+00	3.06113E-02	8.93183E-03	3.98751E-01	1.66363E+00
1461	1.00037E+00	1.00000E+00	4.87613E+03	5.39924E-08	1.66645E+04	7.16546E+05	9.55934E-04
	1.31367E+00	3.85143E+33	0.00000E+00	2.49867E-02	5.62273E-03	3.98696E-01	1.66351E+00
1481	1.00042E+00	1.00000E+00	4.87021E+03	4.12655E-08	1.27213E+04	7.16082E+05	9.61952E-04
	1.31367E+00	3.85143E+33	0.00000E+00	2.04593E-02	3.53164E-03	3.98613E-01	1.66333E+00
1501	1.00046E+00	1.00000E+00	4.86647E+03	3.14434E-08	9.68632E+03	7.15762E+05	9.65581E-04
	1.31366E+00	3.85143E+33	0.00000E+00	1.67913E-02	2.21376E-03	3.98491E-01	1.66306E+00
1521	1.00051E+00	1.00000E+00	4.86410E+03	2.38867E-08	7.35522E+03	7.15520E+05	9.67638E-04
	1.31366E+00	3.85143E+33	0.00000E+00	1.38075E-02	1.38498E-03	3.98316E-01	1.66266E+00
1541	1.00055E+00	1.00000E+00	4.86261E+03	1.80872E-08	5.56809E+03	7.15313E+05	9.68631E-04
	1.31365E+00	3.85143E+33	0.00000E+00	1.13742E-02	8.64760E-04	3.98067E-01	1.66210E+00
1561	1.00060E+00	1.00000E+00	4.86166E+03	1.36460E-08	4.20042E+03	7.15108E+05	9.68862E-04
	1.31365E+00	3.85143E+33	0.00000E+00	9.38651E-03	5.38765E-04	3.97724E-01	1.66133E+00
1581	1.00064E+00	1.00000E+00	4.86107E+03	1.02519E-08	3.15565E+03	7.14881E+05	9.68521E-04
	1.31364E+00	3.85143E+33	0.00000E+00	7.76067E-03	3.34815E-04	3.97261E-01	1.66029E+00

TABLE 3A—*Continued*

Shell	Radius Frac	Mass Frac	Temperature	Density	Pressure	Sound Speed	Brunt V Sq
	Mean Mol Wt	Luminosity	Nuc Rate	Opacity	Temp Grad	Ad Temp Grad	Gamma 1
1601	1.00069E+00	1.00000E+00	4.86069E+03	7.66917E-09	2.36083E+03	7.14615E+05	9.68026E-04
	1.31364E+00	3.85143E+33	0.00000E+00	6.46258E-03	2.08651E-04	3.96649E-01	1.65892E+00
1621	1.00074E+00	1.00000E+00	4.86046E+03	5.71564E-09	1.75975E+03	7.14296E+05	9.66896E-04
	1.31363E+00	3.85143E+33	0.00000E+00	5.40091E-03	1.30003E-04	3.95859E-01	1.65718E+00
1641	1.00079E+00	1.00000E+00	4.86031E+03	4.24287E-09	1.30664E+03	7.13914E+05	9.65380E-04
	1.31362E+00	3.85143E+33	0.00000E+00	4.52840E-03	8.09451E-05	3.94853E-01	1.65498E+00
1661	1.00083E+00	1.00000E+00	4.86021E+03	3.13629E-09	9.66214E+02	7.13460E+05	9.63485E-04
	1.31361E+00	3.85143E+33	0.00000E+00	3.80979E-03	5.03613E-05	3.93589E-01	1.65227E+00
1681	1.00088E+00	1.00000E+00	4.86015E+03	2.30775E-09	7.11331E+02	7.12927E+05	9.61204E-04
	1.31360E+00	3.85143E+33	0.00000E+00	3.21665E-03	3.13054E-05	3.92009E-01	1.64895E+00
1701	1.00093E+00	1.00000E+00	4.86011E+03	1.68965E-09	5.21190E+02	7.12311E+05	9.58525E-04
	1.31358E+00	3.85143E+33	0.00000E+00	2.72599E-03	1.94392E-05	3.90042E-01	1.64490E+00
1721	1.00099E+00	1.00000E+00	4.86009E+03	1.23030E-09	3.79886E+02	7.11607E+05	9.55432E-04
	1.31356E+00	3.85143E+33	0.00000E+00	2.31917E-03	1.20546E-05	3.87590E-01	1.63999E+00
1741	1.00104E+00	1.00000E+00	4.86007E+03	8.90109E-10	2.75235E+02	7.10815E+05	9.51409E-04
	1.31354E+00	3.85143E+33	0.00000E+00	1.97459E-03	7.43622E-06	3.84521E-01	1.63400E+00
1761	1.00109E+00	1.00000E+00	4.86007E+03	6.37442E-10	1.97510E+02	7.09934E+05	9.47169E-04
	1.31351E+00	3.85143E+33	0.00000E+00	1.67668E-03	4.53122E-06	3.80625E-01	1.62662E+00
1781	1.00115E+00	1.00000E+00	4.86006E+03	4.49969E-10	1.39839E+02	7.08979E+05	9.42409E-04
	1.31348E+00	3.85143E+33	0.00000E+00	1.42824E-03	2.73280E-06	3.75601E-01	1.61741E+00
1801	1.00121E+00	1.00000E+00	4.86006E+03	3.11347E-10	9.71959E+01	7.08004E+05	9.37237E-04
	1.31343E+00	3.85143E+33	0.00000E+00	1.22118E-03	1.62408E-06	3.69015E-01	1.60571E+00
1821	1.00127E+00	1.00000E+00	4.86005E+03	2.09267E-10	6.57928E+01	7.07156E+05	9.32076E-04
	1.31337E+00	3.85143E+33	0.00000E+00	1.04891E-03	9.44271E-07	3.60204E-01	1.59057E+00

convection zone. The solar surface lithium abundance is depleted by a factor of 200 with respect to the meteoric value (e.g., see the list of abundances in Anders & Grevesse 1989). During the pre–main-sequence phase of evolution, the solar surface convection zone is much deeper and hotter at the base than it is today. Prior evolutionary calculations (e.g., Bodenheimer 1965) indicated that the amount of pre–main-sequence depletion of Li in solar models is insufficient to explain the observed degree of depletion, thus creating a solar "lithium problem," which sparked a number of investigations into potential lithium depletion mechanisms. The higher opacities in our improved solar model cause a deeper surface convection zone than is present in older models, which might imply increased depletion during the pre–main-sequence phases. *However*, lithium burning in the pre–main-sequence cannot be the sole source for the observed solar lithium depletion because stellar observations place strong constraints on the timing of lithium depletion in solar-type stars (see Pinsonneault et al. 1989, 1990). The observed lithium abundances are relatively high in young open cluster G stars (post–zero-age main-sequence stars) and progressively decrease with increased age; this implies that, in addition to pre–main-sequence depletion, a main-sequence depletion mechanism (not present in standard solar models) is needed.

The effect of the equation-of-state modifications on Γ_1 are shown in Figure 1. Γ_1 for both the STD model and the Ross-Aller model are identical; hence Γ_1 for the MHD equation-of-state model can be directly compared to the STD model. Here we can see that indeed, as concluded by Christensen-Dalsgaard et al. (1988), the dominant correction to the ideal gas equation of state is the Debye-Hückel correction, at least in the deep interior. At lower temperatures and densities, as one approaches the surface conection zone, the Debye-Hückel correction we have applied (which assumes full ionization of all species) does not fit the MHD equation of state. The MHD equation of state does include a Debye-Hückel correction (for full *and* partially ionized ions) to take into account Coulomb interactions of the ions and electrons, but apparently there are other effects or corrections, equally important, possibly partial ionization, which affect Γ_1 in exactly the opposite manner to that of the fully ionized Debye-Hückel correction we have used.

The relative opacity differences with respect to the STD model are shown in Figure 2. The OPAL opacities are 30%

TABLE 3B

SUMMARY OF COMBINED MODEL

Shell	Radius Frac	Mass Frac	Temperature	Density	Pressure	Sound Speed	Brunt V Sq
	Mean Mol Wt	Luminosity	Nuc Rate	Opacity	Temp Grad	Ad Temp Grad	Gamma 1
1	6.53350E-03	2.97851E-05	1.57209E+07	1.50466E+02	2.33481E+17	5.07986E+07	1.26968E-07
	8.59825E-01	1.01853E+30	1.77485E+01	1.28991E+00	3.34189E-01	3.98264E-01	1.66300E+00
21	2.24504E-02	1.18576E-03	1.55637E+07	1.45511E+02	2.26582E+17	5.08882E+07	1.38316E-06
	8.48041E-01	3.97618E+31	1.70313E+01	1.30539E+00	3.35046E-01	3.98287E-01	1.66304E+00
41	6.16068E-02	2.15380E-02	1.45774E+07	1.18048E+02	1.86181E+17	5.12186E+07	6.25333E-06
	7.83050E-01	6.20462E+32	1.30174E+01	1.40810E+00	3.31495E-01	3.98418E-01	1.66333E+00
61	8.89534E-02	5.67163E-02	1.35837E+07	9.57266E+01	1.50244E+17	5.10985E+07	8.03229E-06
	7.32255E-01	1.39050E+33	9.61160E+00	1.52349E+00	3.26695E-01	3.98541E-01	1.66360E+00
81	1.14635E-01	1.05361E-01	1.25670E+07	7.71027E+01	1.18090E+17	5.04813E+07	8.85445E-06
	6.93365E-01	2.16121E+33	6.65358E+00	1.65584E+00	3.18738E-01	3.98657E-01	1.66385E+00
101	1.46205E-01	1.81946E-01	1.13214E+07	5.84469E+01	8.44187E+16	4.90267E+07	7.37328E-06
	6.61390E-01	2.93230E+33	3.77266E+00	1.84268E+00	3.02463E-01	3.98785E-01	1.66413E+00
121	1.84971E-01	2.92302E-01	9.90618E+06	4.08477E+01	5.32282E+16	4.65712E+07	6.88369E-06
	6.40260E-01	3.49394E+33	1.61770E+00	2.11106E+00	2.76454E-01	3.98909E-01	1.66441E+00
141	2.20574E-01	3.99003E-01	8.77021E+06	2.87196E+01	3.35364E+16	4.40885E+07	7.05329E-06
	6.31371E-01	3.72355E+33	6.74338E-01	2.39728E+00	2.51360E-01	3.98990E-01	1.66461E+00
161	2.54275E-01	4.96311E-01	7.84642E+06	2.01457E+01	2.11348E+16	4.17909E+07	7.25614E-06
	6.27644E-01	3.81177E+33	2.89267E-01	2.72891E+00	2.31630E-01	3.99035E-01	1.66474E+00
181	2.86966E-01	5.82162E-01	7.07660E+06	1.40667E+01	1.33214E+16	3.97066E+07	7.25118E-06
	6.26071E-01	3.84249E+33	8.26555E-02	3.11643E+00	2.16570E-01	3.99050E-01	1.66483E+00
201	3.19270E-01	6.56311E-01	6.42033E+06	9.77621E+00	8.39743E+15	3.78162E+07	6.97305E-06
	6.25402E-01	3.84911E+33	2.44382E-02	3.58345E+00	2.05868E-01	3.99043E-01	1.66487E+00
221	3.51632E-01	7.19426E-01	5.84930E+06	6.76948E+00	5.29389E+15	3.60829E+07	6.48362E-06
	6.25116E-01	3.85100E+33	9.88234E-03	4.13363E+00	1.98335E-01	3.99018E-01	1.66488E+00
241	3.84379E-01	7.72573E-01	5.34513E+06	4.67355E+00	3.33755E+15	3.44809E+07	5.90005E-06
	6.24993E-01	3.85159E+33	4.06990E-03	4.77145E+00	1.92781E-01	3.98976E-01	1.66486E+00
261	4.17759E-01	8.16952E-01	4.89471E+06	3.21983E+00	2.10425E+15	3.29849E+07	5.25799E-06
	6.24941E-01	3.85173E+33	1.66593E-03	5.52386E+00	1.89240E-01	3.98916E-01	1.66481E+00
281	4.51951E-01	8.53749E-01	4.48744E+06	2.21544E+00	1.32673E+15	3.15742E+07	4.61557E-06
	6.24919E-01	3.85173E+33	6.74315E-04	6.41722E+00	1.87751E-01	3.98840E-01	1.66473E+00
301	4.87079E-01	8.84067E-01	4.11533E+06	1.52375E+00	8.36532E+14	3.02302E+07	4.00116E-06
	6.24910E-01	3.85169E+33	2.68740E-04	7.45926E+00	1.87865E-01	3.98749E-01	1.66462E+00
321	5.23208E-01	9.08899E-01	3.77243E+06	1.04840E+00	5.27462E+14	2.89384E+07	3.43638E-06
	6.24904E-01	3.85165E+33	1.04992E-04	8.68140E+00	1.89910E-01	3.98645E-01	1.66450E+00
341	5.60338E-01	9.29114E-01	3.45233E+06	7.22485E-01	3.32591E+14	2.76800E+07	2.90728E-06
	6.24904E-01	3.85161E+33	3.98931E-05	1.01514E+01	1.95291E-01	3.98534E-01	1.66437E+00
361	5.98377E-01	9.45463E-01	3.14825E+06	4.99638E-01	2.09719E+14	2.64302E+07	2.41202E-06
	6.24903E-01	3.85158E+33	0.00000E+00	1.19245E+01	2.05549E-01	3.98427E-01	1.66425E+00
381	6.37092E-01	9.58587E-01	2.85286E+06	3.47708E-01	1.32243E+14	2.51580E+07	1.93230E-06
	6.24903E-01	3.85155E+33	0.00000E+00	1.40562E+01	2.23484E-01	3.98346E-01	1.66416E+00

TABLE 3B—*Continued*

Shell	Radius Frac	Mass Frac	Temperature	Density	Pressure	Sound Speed	Brunt V Sq
	Mean Mol Wt	Luminosity	Nuc Rate	Opacity	Temp Grad	Ad Temp Grad	Gamma 1
401	6.76044E-01	9.69025E-01	2.55583E+06	2.44761E-01	8.33901E+13	2.38113E+07	1.40566E-06
	6.24903E-01	3.85153E+33	0.00000E+00	1.66892E+01	2.56943E-01	3.98329E-01	1.66415E+00
421	7.14407E-01	9.77228E-01	2.23441E+06	1.76578E-01	5.25855E+13	2.22632E+07	5.09837E-07
	6.24903E-01	3.85152E+33	0.00000E+00	2.08314E+01	3.43312E-01	3.98458E-01	1.66436E+00
441	7.50661E-01	9.83591E-01	1.86448E+06	1.33163E-01	3.30816E+13	2.03371E+07	-9.75953E-12
	6.24903E-01	3.85150E+33	0.00000E+00	2.98941E+01	3.98803E-01	3.98803E-01	1.66486E+00
461	7.83360E-01	9.88359E-01	1.55130E+06	1.00963E-01	2.08645E+13	1.85509E+07	-9.95317E-12
	6.24903E-01	3.85149E+33	0.00000E+00	4.06848E+01	3.99081E-01	3.99081E-01	1.66527E+00
481	8.12679E-01	9.91869E-01	1.29062E+06	7.65575E-02	1.31601E+13	1.69208E+07	-1.13530E-11
	6.24903E-01	3.85149E+33	0.00000E+00	5.34144E+01	3.99296E-01	3.99295E-01	1.66559E+00
501	8.38708E-01	9.94400E-01	1.07368E+06	5.80561E-02	8.30122E+12	1.54334E+07	-1.39314E-11
	6.24903E-01	3.85149E+33	0.00000E+00	6.92420E+01	3.99459E-01	3.99458E-01	1.66583E+00
521	8.61609E-01	9.96191E-01	8.93164E+05	4.40330E-02	5.23651E+12	1.40757E+07	-1.13460E-08
	6.24650E-01	3.85148E+33	0.00000E+00	7.50643E+01	3.99579E-01	3.99578E-01	1.66602E+00
541	8.81589E-01	9.97437E-01	7.42984E+05	3.34386E-02	3.30339E+12	1.28295E+07	-5.98949E-08
	6.25468E-01	3.85148E+33	0.00000E+00	1.02292E+02	3.99574E-01	3.99573E-01	1.66614E+00
561	8.98870E-01	9.98292E-01	6.18101E+05	2.54378E-02	2.08397E+12	1.16830E+07	-1.11765E-07
	6.27425E-01	3.85148E+33	0.00000E+00	1.43309E+02	3.99290E-01	3.99289E-01	1.66610E+00
581	9.13703E-01	9.98872E-01	5.14329E+05	1.93681E-02	1.31472E+12	1.06332E+07	-1.32855E-07
	6.30071E-01	3.85148E+33	0.00000E+00	2.08086E+02	3.98583E-01	3.98581E-01	1.66566E+00
601	9.26366E-01	9.99260E-01	4.28173E+05	1.47366E-02	8.29446E+11	9.67931E+06	-1.01382E-07
	6.32572E-01	3.85148E+33	0.00000E+00	3.32963E+02	3.97363E-01	3.97360E-01	1.66455E+00
621	9.37140E-01	9.99517E-01	3.56696E+05	1.11905E-02	5.23298E+11	8.81731E+06	-2.93135E-08
	6.34267E-01	3.85148E+33	0.00000E+00	5.97177E+02	3.95592E-01	3.95587E-01	1.66255E+00
641	9.46291E-01	9.99687E-01	2.97445E+05	8.48187E-03	3.30154E+11	8.03616E+06	-1.40331E-10
	6.35397E-01	3.85148E+33	0.00000E+00	1.08507E+03	3.92972E-01	3.92964E-01	1.65909E+00
661	9.54078E-01	9.99798E-01	2.48258E+05	6.41194E-03	2.07802E+11	7.31798E+06	-2.79704E-10
	6.36940E-01	3.85148E+33	0.00000E+00	1.90831E+03	3.88401E-01	3.88390E-01	1.65242E+00
681	9.60638E-01	9.99870E-01	2.07941E+05	4.84780E-03	1.31114E+11	6.66002E+06	-4.57088E-10
	6.39273E-01	3.85148E+33	0.00000E+00	3.19603E+03	3.80569E-01	3.80555E-01	1.64000E+00
701	9.66189E-01	9.99916E-01	1.74971E+05	3.65495E-03	8.27277E+10	6.05440E+06	-7.71869E-10
	6.42757E-01	3.85148E+33	0.00000E+00	5.08558E+03	3.68445E-01	3.68425E-01	1.61947E+00
721	9.70893E-01	9.99946E-01	1.48174E+05	2.74390E-03	5.21977E+10	5.50386E+06	-1.33862E-09
	6.47644E-01	3.85148E+33	0.00000E+00	7.55044E+03	3.53313E-01	3.53286E-01	1.59239E+00
741	9.74891E-01	9.99965E-01	1.26330E+05	2.04989E-03	3.29345E+10	5.01842E+06	-2.28912E-09
	6.53781E-01	3.85148E+33	0.00000E+00	1.16738E+04	3.40260E-01	3.40224E-01	1.56752E+00
761	9.78300E-01	9.99978E-01	1.08167E+05	1.52610E-03	2.07802E+10	4.60431E+06	-3.79288E-09
	6.60502E-01	3.85148E+33	0.00000E+00	1.84834E+04	3.35643E-01	3.35591E-01	1.55691E+00
781	9.81209E-01	9.99986E-01	9.25856E+04	1.13607E-03	1.31114E+10	4.25184E+06	-6.12356E-09
	6.67023E-01	3.85148E+33	0.00000E+00	2.90005E+04	3.41222E-01	3.41147E-01	1.56642E+00

TABLE 3B—*Continued*

Shell	Radius Frac	Mass Frac	Temperature	Density	Pressure	Sound Speed	Brunt V Sq
	Mean Mol Wt	Luminosity	Nuc Rate	Opacity	Temp Grad	Ad Temp Grad	Gamma 1
801	9.83685E-01	9.99991E-01	7.89767E+04	8.48154E-04	8.27277E+09	3.92983E+06	-9.92831E-09
	6.73231E-01	3.85148E+33	0.00000E+00	4.10897E+04	3.48151E-01	3.48041E-01	1.58333E+00
821	9.85785E-01	9.99994E-01	6.73234E+04	6.34256E-04	5.21977E+09	3.60614E+06	-1.65477E-08
	6.80174E-01	3.85148E+33	0.00000E+00	5.08225E+04	3.42337E-01	3.42185E-01	1.58015E+00
841	9.87566E-01	9.99996E-01	5.77591E+04	4.72705E-04	3.29345E+09	3.28395E+06	-2.71266E-08
	6.89287E-01	3.85148E+33	0.00000E+00	5.85515E+04	3.21049E-01	3.20852E-01	1.54786E+00
861	9.89084E-01	9.99997E-01	5.01474E+04	3.49507E-04	2.07802E+09	2.98674E+06	-4.29377E-08
	7.01283E-01	3.85148E+33	0.00000E+00	6.73448E+04	2.92222E-01	2.91976E-01	1.50038E+00
881	9.90390E-01	9.99998E-01	4.41216E+04	2.55900E-04	1.31114E+09	2.72929E+06	-6.63757E-08
	7.15996E-01	3.85148E+33	0.00000E+00	7.79717E+04	2.64428E-01	2.64124E-01	1.45385E+00
901	9.91523E-01	9.99999E-01	3.92749E+04	1.85658E-04	8.27277E+08	2.51213E+06	-1.01745E-07
	7.32856E-01	3.85148E+33	0.00000E+00	8.69601E+04	2.41907E-01	2.41526E-01	1.41627E+00
921	9.92514E-01	9.99999E-01	3.52804E+04	1.33702E-04	5.21977E+08	2.32783E+06	-1.55898E-07
	7.51382E-01	3.85148E+33	0.00000E+00	9.01018E+04	2.24641E-01	2.24157E-01	1.38800E+00
941	9.93387E-01	9.99999E-01	3.19186E+04	9.57245E-05	3.29345E+08	2.16762E+06	-2.38742E-07
	7.71358E-01	3.85148E+33	0.00000E+00	8.55861E+04	2.10603E-01	2.09980E-01	1.36565E+00
961	9.94159E-01	9.99999E-01	2.90542E+04	6.81907E-05	2.07802E+08	2.02494E+06	-3.64065E-07
	7.92728E-01	3.85148E+33	0.00000E+00	6.81365E+04	1.97851E-01	1.97052E-01	1.34555E+00
981	9.94845E-01	9.99999E-01	2.65993E+04	4.83421E-05	1.31114E+08	1.89634E+06	-5.51456E-07
	8.15428E-01	3.85148E+33	0.00000E+00	5.10734E+04	1.85635E-01	1.84609E-01	1.32590E+00
1001	9.95459E-01	9.99999E-01	2.44854E+04	3.41060E-05	8.27277E+07	1.78033E+06	-8.29924E-07
	8.39322E-01	3.85148E+33	0.00000E+00	2.91427E+04	1.74150E-01	1.72833E-01	1.30672E+00
1021	9.96009E-01	9.99999E-01	2.26534E+04	2.39501E-05	5.21977E+07	1.67586E+06	-1.24305E-06
	8.64238E-01	3.85148E+33	0.00000E+00	2.08171E+04	1.63791E-01	1.62090E-01	1.28865E+00
1041	9.96505E-01	9.99999E-01	2.10523E+04	1.67461E-05	3.29345E+07	1.58173E+06	-1.85608E-06
	8.90036E-01	3.85148E+33	0.00000E+00	1.47953E+04	1.54776E-01	1.52560E-01	1.27212E+00
1061	9.96954E-01	9.99999E-01	1.96395E+04	1.16647E-05	2.07802E+07	1.49659E+06	-2.76647E-06
	9.16638E-01	3.85148E+33	0.00000E+00	1.03648E+04	1.47160E-01	1.44242E-01	1.25727E+00
1081	9.97362E-01	9.99999E-01	1.83799E+04	8.09947E-06	1.31114E+07	1.41911E+06	-4.12037E-06
	9.44051E-01	3.85148E+33	0.00000E+00	7.28221E+03	1.40936E-01	1.37049E-01	1.24405E+00
1101	9.97733E-01	9.99999E-01	1.72449E+04	5.61010E-06	8.27277E+06	1.34804E+06	-6.13881E-06
	9.72365E-01	3.85148E+33	0.00000E+00	5.08130E+03	1.36121E-01	1.30880E-01	1.23232E+00
1121	9.98072E-01	9.99999E-01	1.62104E+04	3.87950E-06	5.21977E+06	1.28224E+06	-9.16044E-06
	1.00177E+00	3.85148E+33	0.00000E+00	3.52011E+03	1.32821E-01	1.25662E-01	1.22198E+00
1141	9.98382E-01	9.99999E-01	1.52551E+04	2.68108E-06	3.29345E+06	1.22065E+06	-1.37143E-05
	1.03259E+00	3.85148E+33	0.00000E+00	2.41483E+03	1.31296E-01	1.21372E-01	1.21295E+00
1161	9.98664E-01	9.99999E-01	1.43589E+04	1.85408E-06	2.07802E+06	1.16224E+06	-2.06519E-05
	1.06526E+00	3.85148E+33	0.00000E+00	1.62059E+03	1.32081E-01	1.18076E-01	1.20524E+00
1181	9.98922E-01	9.99999E-01	1.35008E+04	1.28523E-06	1.31114E+06	1.10599E+06	-3.14057E-05
	1.10042E+00	3.85148E+33	0.00000E+00	1.05696E+03	1.36227E-01	1.15998E-01	1.19905E+00

TABLE 3B—*Continued*

Shell	Radius Frac Mean Mol Wt	Mass Frac Luminosity	Temperature Nuc Rate	Density Opacity	Pressure Temp Grad	Sound Speed Ad Temp Grad	Brunt V Sq Gamma 1
1201	9.99156E-01	9.99999E-01	1.26552E+04	8.95291E-07	8.27277E+05	1.05079E+06	-4.85665E-05
	1.13881E+00	3.85148E+33	0.00000E+00	6.54960E+02	1.45896E-01	1.15694E-01	1.19495E+00
1221	9.99367E-01	9.99999E-01	1.17847E+04	6.29213E-07	5.21977E+05	9.95444E+05	-7.74141E-05
	1.18125E+00	3.85148E+33	0.00000E+00	3.70209E+02	1.66056E-01	1.18577E-01	1.19448E+00
1241	9.99556E-01	1.00000E+00	1.08215E+04	4.49449E-07	3.29345E+05	9.38751E+05	-1.31286E-04
	1.22800E+00	3.85148E+33	0.00000E+00	1.74731E+02	2.10517E-01	1.28836E-01	1.20262E+00
1261	9.99720E-01	1.00000E+00	9.60036E+03	3.32288E-07	2.07802E+05	8.81207E+05	-2.61656E-04
	1.27653E+00	3.85148E+33	0.00000E+00	5.44627E+01	3.33022E-01	1.63451E-01	1.24171E+00
1281	9.99855E-01	1.00000E+00	7.51707E+03	2.75230E-07	1.31114E+05	8.38158E+05	-8.47450E-04
	1.31207E+00	3.85148E+33	0.00000E+00	4.28404E+00	8.34263E-01	3.12555E-01	1.47467E+00
1301	9.99955E-01	1.00000E+00	6.01409E+03	2.17658E-07	8.27277E+04	7.88937E+05	3.33897E-04
	1.31567E+00	3.85148E+33	0.00000E+00	4.55066E-01	2.19682E-01	3.88309E-01	1.63760E+00
1321	1.00001E+00	1.00000E+00	5.65458E+03	1.68426E-07	6.01828E+04	7.68260E+05	3.30726E-04
	1.31581E+00	3.85148E+33	0.00000E+00	2.52854E-01	1.13629E-01	3.94078E-01	1.65179E+00
1341	1.00005E+00	1.00000E+00	5.39372E+03	1.40977E-07	4.80489E+04	7.51900E+05	4.64080E-04
	1.31586E+00	3.85148E+33	0.00000E+00	1.80657E-01	7.82954E-02	3.96858E-01	1.65877E+00
1361	1.00010E+00	1.00000E+00	5.18272E+03	1.15348E-07	3.77755E+04	7.37755E+05	5.76318E-04
	1.31588E+00	3.85148E+33	0.00000E+00	1.39889E-01	5.59129E-02	3.98119E-01	1.66198E+00
1381	1.00014E+00	1.00000E+00	5.01998E+03	9.32159E-08	2.95685E+04	7.26345E+05	6.74599E-04
	1.31589E+00	3.85148E+33	0.00000E+00	1.11974E-01	3.98007E-02	3.98591E-01	1.66320E+00
1401	1.00018E+00	1.00000E+00	4.89888E+03	7.46823E-08	2.31182E+04	7.17621E+05	7.61561E-04
	1.31590E+00	3.85148E+33	0.00000E+00	8.99715E-02	2.75690E-02	3.98747E-01	1.66362E+00
1421	1.00022E+00	1.00000E+00	4.81160E+03	5.93823E-08	1.80547E+04	7.11232E+05	8.34514E-04
	1.31590E+00	3.85148E+33	0.00000E+00	7.23767E-02	1.86114E-02	3.98790E-01	1.66375E+00
1441	1.00026E+00	1.00000E+00	4.75064E+03	4.69280E-08	1.40875E+04	7.06723E+05	8.91851E-04
	1.31590E+00	3.85148E+33	0.00000E+00	5.83580E-02	1.23218E-02	3.98791E-01	1.66378E+00
1461	1.00030E+00	1.00000E+00	4.70922E+03	3.69194E-08	1.09866E+04	7.03641E+05	9.34385E-04
	1.31590E+00	3.85148E+33	0.00000E+00	4.71687E-02	8.04398E-03	3.98775E-01	1.66376E+00
1481	1.00034E+00	1.00000E+00	4.68172E+03	2.89623E-08	8.56864E+03	7.01586E+05	9.64394E-04
	1.31590E+00	3.85148E+33	0.00000E+00	3.82018E-02	5.20143E-03	3.98748E-01	1.66373E+00
1501	1.00037E+00	1.00000E+00	4.66376E+03	2.26827E-08	6.68533E+03	7.00242E+05	9.84812E-04
	1.31590E+00	3.85148E+33	0.00000E+00	3.09461E-02	3.33836E-03	3.98709E-01	1.66368E+00
1521	1.00041E+00	1.00000E+00	4.65217E+03	1.77470E-08	5.21789E+03	6.99371E+05	9.98346E-04
	1.31590E+00	3.85148E+33	0.00000E+00	2.50464E-02	2.12994E-03	3.98652E-01	1.66359E+00
1541	1.00045E+00	1.00000E+00	4.64475E+03	1.38756E-08	4.07338E+03	6.98809E+05	1.00714E-03
	1.31589E+00	3.85148E+33	0.00000E+00	2.02540E-02	1.35321E-03	3.98572E-01	1.66347E+00
1561	1.00049E+00	1.00000E+00	4.64003E+03	1.08431E-08	3.18017E+03	6.98442E+05	1.01275E-03
	1.31589E+00	3.85148E+33	0.00000E+00	1.63714E-02	8.57440E-04	3.98457E-01	1.66327E+00
1581	1.00053E+00	1.00000E+00	4.63703E+03	8.46963E-09	2.48270E+03	6.98193E+05	1.01617E-03
	1.31589E+00	3.85148E+33	0.00000E+00	1.32218E-02	5.42010E-04	3.98294E-01	1.66299E+00

TABLE 3B—*Continued*

Shell	Radius Frac Mean Mol Wt	Mass Frac Luminosity	Temperature Nuc Rate	Density Opacity	Pressure Temp Grad	Sound Speed Ad Temp Grad	Brunt V Sq Gamma 1
1601	1.00056E+00	1.00000E+00	4.63513E+03	6.61117E-09	1.93740E+03	6.98011E+05	1.01814E-03
	1.31588E+00	3.85148E+33	0.00000E+00	1.06607E-02	3.41593E-04	3.98067E-01	1.66258E+00
1621	1.00060E+00	1.00000E+00	4.63393E+03	5.15424E-09	1.51031E+03	6.97861E+05	1.01914E-03
	1.31588E+00	3.85148E+33	0.00000E+00	8.58063E-03	2.14555E-04	3.97757E-01	1.66201E+00
1641	1.00064E+00	1.00000E+00	4.63317E+03	4.01064E-09	1.17528E+03	6.97720E+05	1.01947E-03
	1.31588E+00	3.85148E+33	0.00000E+00	6.89729E-03	1.34294E-04	3.97342E-01	1.66124E+00
1661	1.00068E+00	1.00000E+00	4.63269E+03	3.11246E-09	9.12247E+02	6.97568E+05	1.01935E-03
	1.31587E+00	3.85148E+33	0.00000E+00	5.54312E-03	8.38077E-05	3.96791E-01	1.66022E+00
1681	1.00072E+00	1.00000E+00	4.63238E+03	2.40730E-09	7.05788E+02	6.97394E+05	1.01879E-03
	1.31587E+00	3.85148E+33	0.00000E+00	4.45703E-03	5.21496E-05	3.96070E-01	1.65887E+00
1701	1.00076E+00	1.00000E+00	4.63219E+03	1.85394E-09	5.43796E+02	6.97186E+05	1.01783E-03
	1.31586E+00	3.85148E+33	0.00000E+00	3.58426E-03	3.23175E-05	3.95135E-01	1.65713E+00
1721	1.00080E+00	1.00000E+00	4.63207E+03	1.41971E-09	4.16690E+02	6.96938E+05	1.01653E-03
	1.31586E+00	3.85148E+33	0.00000E+00	2.88229E-03	1.99158E-05	3.93925E-01	1.65491E+00
1741	1.00084E+00	1.00000E+00	4.63200E+03	1.07913E-09	3.17005E+02	6.96641E+05	1.01493E-03
	1.31585E+00	3.85148E+33	0.00000E+00	2.32072E-03	1.22001E-05	3.92362E-01	1.65207E+00
1761	1.00089E+00	1.00000E+00	4.63195E+03	8.12581E-10	2.38988E+02	6.96293E+05	1.01299E-03
	1.31584E+00	3.85148E+33	0.00000E+00	1.87383E-03	7.42681E-06	3.90335E-01	1.64844E+00
1781	1.00093E+00	1.00000E+00	4.63192E+03	6.04576E-10	1.78109E+02	6.95893E+05	1.01060E-03
	1.31583E+00	3.85148E+33	0.00000E+00	1.51735E-03	4.48207E-06	3.87689E-01	1.64380E+00
1801	1.00098E+00	1.00000E+00	4.63190E+03	4.42684E-10	1.30727E+02	6.95451E+05	1.00772E-03
	1.31582E+00	3.85148E+33	0.00000E+00	1.23155E-03	2.67012E-06	3.84189E-01	1.63780E+00
1821	1.00103E+00	1.00000E+00	4.63189E+03	3.16969E-10	9.39333E+01	6.94993E+05	1.00436E-03
	1.31581E+00	3.85148E+33	0.00000E+00	1.00190E-03	1.56085E-06	3.79463E-01	1.62989E+00
1841	1.00109E+00	1.00000E+00	4.63188E+03	2.19589E-10	6.54325E+01	6.94601E+05	1.00061E-03
	1.31578E+00	3.85148E+33	0.00000E+00	8.17298E-04	8.86940E-07	3.72883E-01	1.61915E+00
1861	1.00115E+00	1.00000E+00	4.63187E+03	1.44393E-10	4.34245E+01	6.94519E+05	9.96961E-04
	1.31575E+00	3.85148E+33	0.00000E+00	6.69186E-04	4.81951E-07	3.63298E-01	1.60391E+00

greater than the LAOL opacities, used in the STD model, near the base of the convection zone. The abrupt drop at $x = 0.85$ is due to the equally abrupt change from OPAL opacities above 10^6 K, where the tables are defined, to the LAOL opacities (below 10^6 K). Note that in order to calculate the relative differences in opacity for this plot, we had to put the opacity data for each model on identical grids in x. This was done using cubic spline interpolation and is the cause of the overshooting at the jump discontinuity in the OPAL opacity model's opacity. In the outermost layers, both Cox and Kurucz opacities depart from the STD model's opacities (Cox & Stewart). The Cox low-temperature opacity tables begin at temperatures below 10^5 K ($x = 0.98$), and the Kurucz opacity tables begin at temperatures below 10^4 K ($x = 0.997$). The Cox low-temperature opacities show a significant bump at $x = 0.99$ and then another sharp rise just above the surface. The Kurucz low-temperature opacities are similar to the Cox opacities, above $x = 0.997$, showing the same sharp rise above the surface.

Tables 3A and B list the basic structural properties of our STD model and the combined model. All entries are in cgs units. The column identified as "Brunt V Sq" is the square of the Brunt-Väisälä frequency, N^2.

3.2. *p-Mode Frequency Comparisons*

We have calculated the adiabatic p-mode frequencies for $l = 0$, 1, 2, and 3 for all of the solar models using DBG's stellar pulsation program. We have focused on the low-l modes because their lower turning points are deeper which makes them more sensitive to the interior structure than higher l

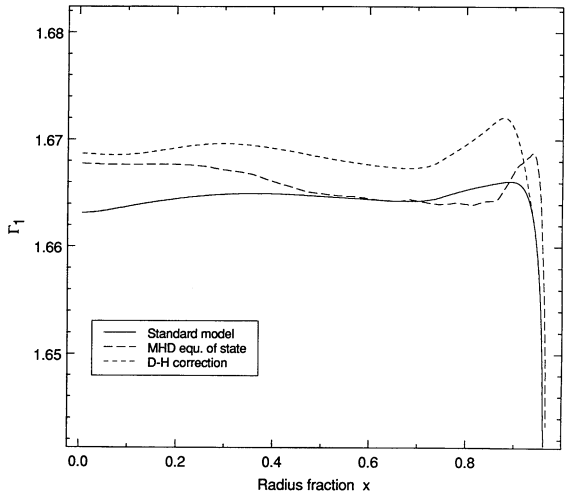

FIG. 1.—Γ_1 is plotted opposite radius fraction x for the standard model (STD), the MHD equation of state model, and the Debye-Hückel correction model. All other models lie on top of the standard model.

modes, whose lower turning points are confined to the upper layers only. The frequencies, the first-order spacings, and the second-order spacings of the STD model and the combined model are listed in Tables 2A and 2B. The 0.000 entry in the $l = 0$ column at $n = 5$ and in the $l = 1$ column at $n = 2$ are artifacts of the radial node number n classification scheme and the development of a steep mean molecular weight gradient in the interior. Because this behavior is not relevant to the model versus Sun comparisons made here, we refer the reader to an extensive discussion of this behavior in Guenther (1991b).

The first-order frequency spacing is defined by

$$\Delta\nu(n, l) \equiv \nu(n, l) - \nu(n - 1, l)$$

and the second-order frequency spacing is defined by

$$\delta\nu(n, l) \equiv \nu(n, l) - \nu(n - 1, l + 2) .$$

The first-order spacing is primarily sensitive to the structure of the very outermost layers ($x > 0.99$), even for low-l modes, and is particularly sensitive to the location of the outer turning point. The second order spacing is primarily sensitive to the structure of the very innermost layers ($x < 0.05$) and is particularly sensitive to the location of the inner turning point. For a detailed discussion of these sensitivities, in the context of 1 $M_\odot$ stellar models, see Guenther (1991b).

In Figures 3*a*–3*h*, we show the relative differences between the frequencies of the solar model and those of the Sun for $l = 0$, 1, 2, and 3. The observed frequencies were taken from the tables of Libbrecht et al. (1990) which contain the low-l results of Jiménez et al. (1987). For plotting and logistic purposes we have divided the models into two sets: the first set, displayed on the left, contains the STD model, the Ross-Aller mixture model, the MHD equation of state model, the Debye-Hückel correction model, and the Cox low-temperature opacities model; and the second set, displayed on the right, contains the Bahcall nuclear reaction rates model, the Krishna Swamy model, the Kurucz low-temperature opacities model, the OPAL opacities model, and the combined model. The combined model includes all of the effects modeled in the second set of models. In Figure 3 the data for the STD model are plotted in both sets of figures for reference. Based on Figure 3, we draw attention to the following results.

1. The largest effect on the frequencies, of the order of ± 5 to ± 10 μHz, is produced by the different opacities.
2. Arguably the best model, with respect to matching the observations, is the combined model.
3. Modifications which do not affect the surface layers tend to increase or decrease all of the frequencies by approximately the same amount, whereas modifications which do affect the surface layers, i.e., Krishna Swamy atmosphere and low-temperature opacities, tend to perturb the frequencies of the high-n modes more than the low-n modes, hence, affect the first-order frequency spacing.
4. The effect of the Debye-Hückel correction on the p-mode frequencies is in the same direction as the MHD equation's effect, but because the Debye-Hückel correction is not applied in the outer regions, it does not have as large an effect on the p-mode frequencies.
5. When the individual modifications are combined, their effect on the p-mode frequencies is additive. The frequencies of the combined model, for example, could have been calculated

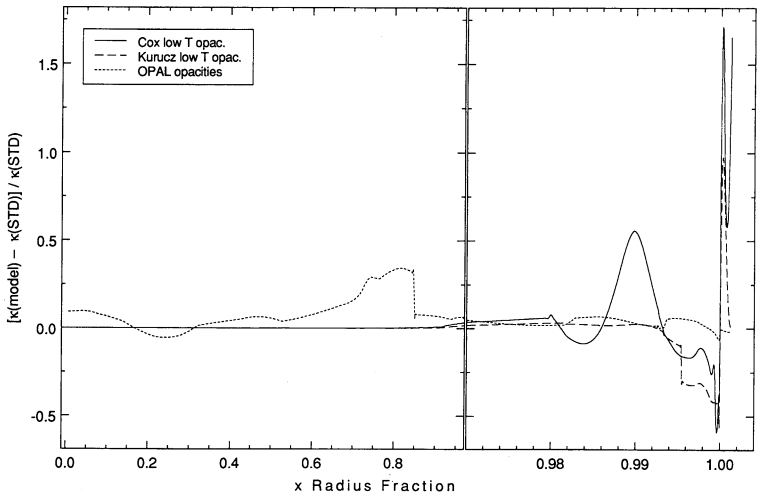

FIG. 2.—The relative differences in the run of opacity are plotted, with respect to the standard model (STD), for the Cox low-temperature "molecular" opacity model, the Kurucz low-temperature "molecular" opacity model, and the Iglesias & Rogers (OPAL) opacity model.

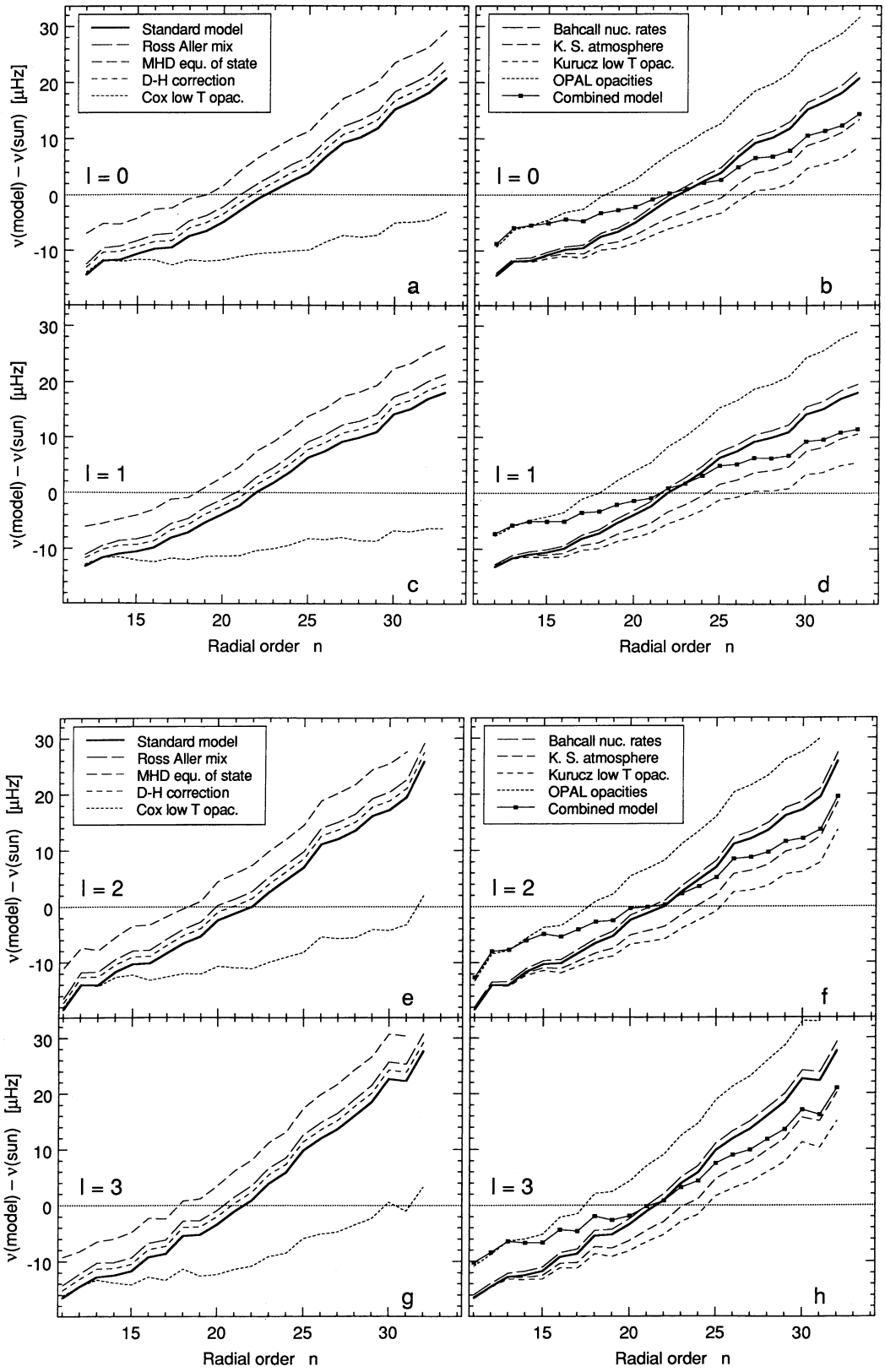

FIG. 3.—The frequencies of the low-l p-modes of the models minus the Sun's low-l p-mode frequencies are plotted opposite the radial order n of the modes. The Ross-Aller mixture model, the MHD equation-of-state model, the Debye-Hückel correction model, and the Cox low-temperature "molecular" opacity model are plotted in the series on the left. The Bahcall nuclear reaction rates model, the Krishna Swamy atmosphere model, the Kurucz low-temperature "molecular" opacity model, the OPAL opacity model, and the combined model are plotted in the series on the right. The combined model includes all the modifications plotted in the right-hand series. The frequencies of STD model, represented by a thick line, are plotted in both series.

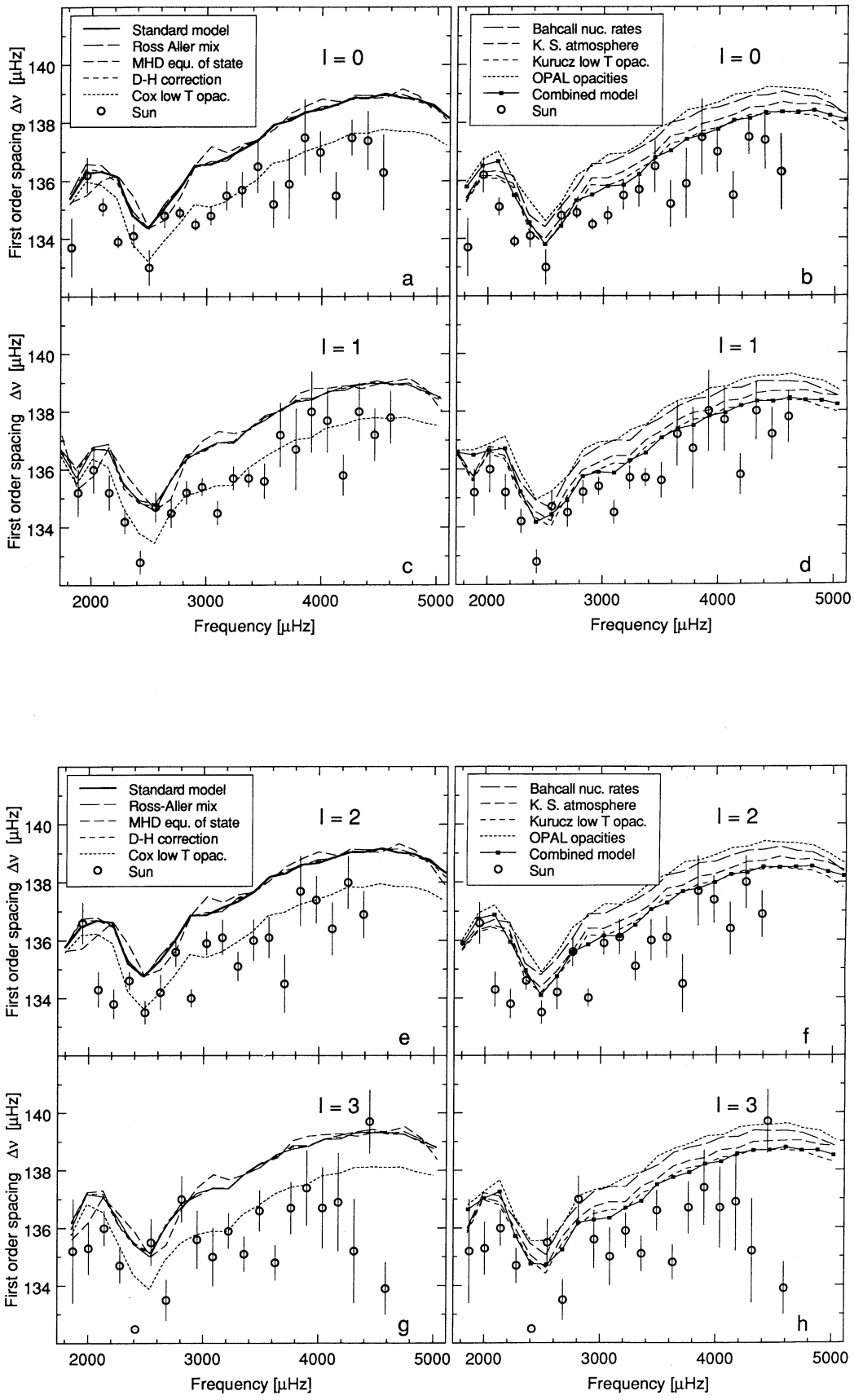

FIG. 4.—The first-order frequency spacings are plotted opposite frequency for the models and the Sun. The plots are divided into two series as described in Fig. 3.

simply by adding the perturbations to the frequencies due to the Krishna Swamy model, the Kurucz model, the OPAL model, and the Bahcall nuclear rates model.

We conclude from Figure 3 that the errors associated with the physics modeled here can introduce up to ± 5 to ± 10 μHz perturbations to the calculated p-mode frequencies of low-l and that the sources of the error, from the set of effects sampled here, in descending order of importance are the low-temperature opacities, the atmosphere model, the equation of state and intermediate temperature opacities, the chemical composition, and the nuclear reaction rates. The combined model falls within the ± 5 to ± 10 μHz errors of the frequencies of the solar model and is, therefore, representative of the best solar model that can be constructed without making use of ad hoc assumptions. Indeed, it is very satisfying that the combined model, using the latest opacities, a reasonable model atmosphere, and a well-determined mixture of elements does fit the observations within understood errors associated with the physics of the model.

Figures 4*a*–4*h* show the first order frequency spacings of the models and the Sun. Here, as noted above, the greatest improvement is obtained from the low-temperature opacities and the Krishna Swamy atmosphere. Once again, the combined model falls satisfyingly close to the observations. A further modification, which we have not done, can be made by including nonadiabatic effects in the oscillation calculations. It is not clear what effect the inclusion of nonadiabatic physics will have on the p-mode frequencies of the models. According to the calculations of Ulrich & Rhodes (1983), the first-order frequency spacings increase by approximately 0.5 μHz (for $l = 0$) when nonadiabatic effects are taken into account. But according to Cox et al. (1989, 1990) the nonadiabatic effects perturb all of the frequencies equally and, thus, should have little effect on the first-order spacings.

Finally, we present the second-order spacings of the models and the Sun in Figures 5*a* and 5*b*. The models are similar enough that they cannot be distinguished in this plot. Only in the frequency range, 2300–4500 μHz for $l = 0$ and 2300–3600 μHz for the $l = 1$ do the second-order spacings match the observations. The large scatter in the observational data at higher frequencies suggests that their error may have been underestimated and that systematic errors exist. If the observational data are correctly represented then, as discussed in Guenther (1991b), the discrepancies imply that the very core of the Sun is less concentrated, and the immediately surrounding regions more concentrated than specified by the standard solar model. We note that the observations of Pallé et al. (1989), are in better agreement with the models for $l = 1$ (see Fig. 6 in their paper) at higher frequencies.

We are reassured that there is now an acceptable and reasonable agreement between the Sun's p-mode spectrum and the spectra of theoretical solar models which include the latest physics, at least with respect to the low-l p-modes; and we note that the agreement is not yet perfect and that there is still work to be done, particularly in the area of opacities and equation of state. Because the opacities and equation-of-state calculations are being improved at this time, our combined model, or any other recipe for a "best" model, is certainly going to improve over the next few years.

4. SUMMARY AND CONCLUSIONS

Recent advances in the basic physics of the solar interior now enable us to construct solar models whose p-mode oscil-

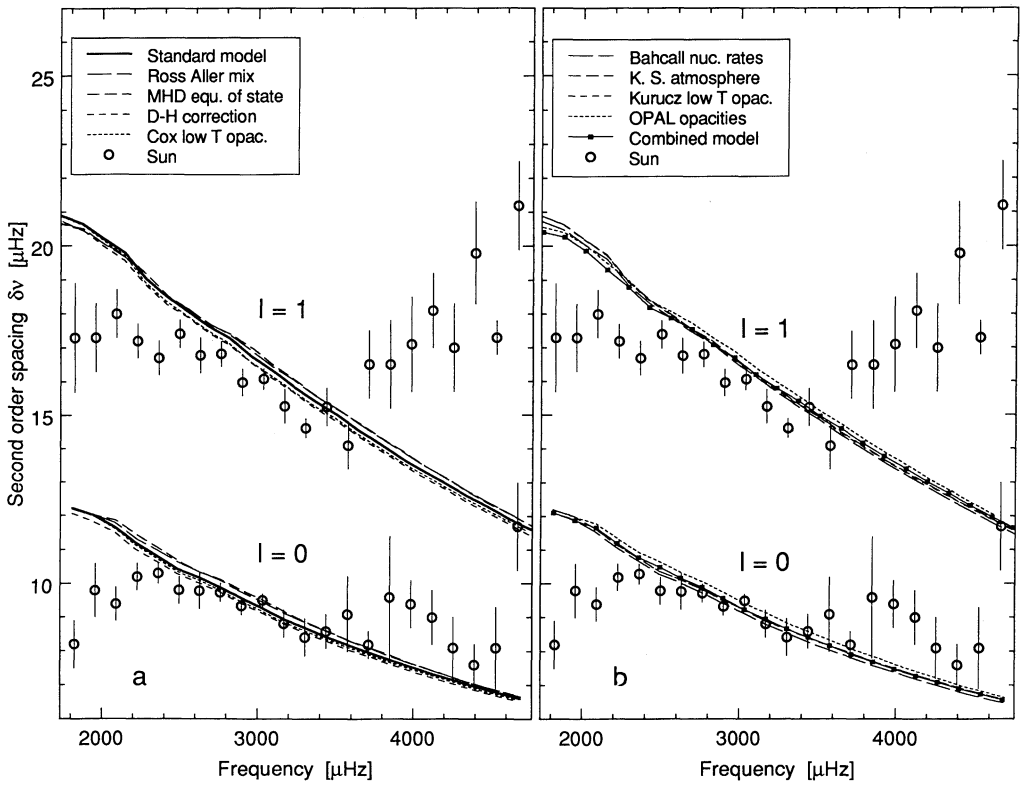

FIG. 5.—The second-order frequency spacings are plotted opposite frequency for the models and the Sun

lation spectrum reproduces the solar low-l p-mode frequencies within $\pm 0.2\%$. More importantly, we can now state with confidence that the remaining discrepancies between our models and observation are at the level which is expected from the known uncertainties in the input physics and solar parameters. In other words, it is no longer necessary to introduce nonstandard or ad hoc assumptions in the models. We emphasize that this statement is an important departure from the conclusion that was first reached by Ulrich & Rhodes (1983), and with which we concurred until recently (see, e.g., Guenther 1991a; Kim et al. 1991), that there is a significant discrepancy between the observed and calculated p-mode spectrum for the Sun, suggesting a possibly serious flaw in our understanding of the Sun's internal structure.

It is worth noting that no single improvement in the physics, when taken individually, necessarily improves the degree of agreement. In other words, no single modification is responsible for resolving the discrepancy between theory and observation. However, two factors dominate in importance: the increased radiative opacities below the convection zone, calculated by Iglesias & Rogers (1991) at Livermore for the Anders & Grevesse (1989) element mixture, which improve markedly the theoretical frequencies, and remove most of the previous discrepancy with the depth of the convection zone, which at $x_{\rm conv} = 0.724 \pm 0.005$ is now close to that derived independently by inversion; and the atmospheric opacities (which include molecular effects) kindly communicated to us by A. N. Cox (1990) and by R. L. Kurucz (1991), which yield the more correct first-order spacings.

With regard to improvements in the equation of state, our results are in agreement with the conclusions of Christensen-Dalsgaard et al. (1988). We note that they also compared the MHD equation of state to another detailed equation of state provided by the OPAL group. Even though the MHD and OPAL equations of state are derived from different formulations they were found to be in very close agreement. The authors suggest that the Debye-Hückel correction (full and partial ionization form) is the dominant correction in the regions in which they made their comparisons. We conclude that our existing equation-of-state formulation is adequate for most stellar evolution calculations and that the fully ionized Debye-Hückel correction (used here) should only be applied in the deep interior, where it does bring the standard ideal gas equation of state in closer agreement with the MHD equation of state.

An important by-product of this solar modeling from the points of view of cosmology and Galactic astronomy is a reliable determination of the initial helium abundance of the Sun. We find $Y = 0.28 \pm 0.01$. This method of determining Y for the Sun is very robust, as it relies primarily on the mass, luminosity, and age of the Sun, all well-determined parameters. Since $L \propto \mu^{7.5}$, where μ is the mean molecular weight of the bulk of the mass of the Sun, the initial Y of the Sun can be derived with precision. Note that if it ever becomes possible to perform the much more difficult task of estimating Y in the outer layer of the Sun by seismic means with sufficient accuracy (see, e.g., Däppen & Gough 1985), it will provide, in addition, information about the efficiency of helium diffusion in the solar envelope. This approach requires the use of p-modes with $l > 3$ and therefore unfortunately could not be used in stars.

In the larger astronomical context, we are now in a position to address with increased confidence the study of the structure and evolution of other Sun-like stars, which have important implications for the chronology of old stars and Galactic evolution. Similarly, neutrino physicists can find the solar interior a more predictable environment for testing neutrino interactions (SAGE and GALLEX experiments; Bahcall 1989).

We believe a major challenge ahead in heliosmology will be the study of the internal dynamics of the Sun. Increased confidence in our understanding of the deep internal structure will facilitate the study of the outer envelope and atmosphere which can also be well studied with higher l modes. An improved solar model should also improve the reliability of inversion procedures; these may in turn eventually reveal the state of the solar internal rotation and other internal motions, although how feasible this objective is for the layers below 0.5 $R_\odot$ is still unclear.

We note that helioseismology is an effective probe of only the outer 10% of the mass of the Sun since 90% of the mass of the Sun is contained in layers below 0.5 $R_\odot$ (2% of the mass of the Sun is in the convection zone). However, much of interest takes place in these outer layers. The study of the structure and dynamics of the convection zone and of the transition region just below, where overshoot takes place, and of the superadiabatic layers in the subphotosphere will be greatly facilitated with the data and deductions provided by helioseismology. Direct comparisons with the detailed numerical modeling of convection currently underway will become increasingly meaningful (Chan & Sofia 1989). Similarly, the connection between the dynamics of the convection zone and the solar activity cycle and activity will be studied and subjected to direct comparisons with increasingly more detailed numerical models (Fox, Theobald, & Sofia 1991). Other observed variations in the solar parameters, which are seated in the convection zone and take place on time scales from year to centuries, will also be amenable to analysis and detailed physical modeling (Endal, Sofia, & Twigg 1985; Endal & Sofia 1981).

One last point must be considered. The g-mode spectrum of the Sun is very sensitive to the structure of the deep interior but, unfortunately, to date, attempts to observe g-modes have either failed or have not stood up to independent verification. Because it may be possible to observe g-modes from space (the GOLF/SOHO experiment, the SDS experiment of Sofia, Maier, & Twigg 1991) or from the global oscillation networks (IRIS, Birmingham, and GONG) now nearing operation, we will discuss the sensitivities of the g-mode spectrum of our models in a separate paper.

We are grateful for the support of this work from NASA grants NAGW-777, NAGW-778, and NAG5-1486.

REFERENCES

Anders, E., & Grevesse, N. 1989, Geochim. Cosmochim. Acta, 53, 197
Bahcall, J. N. 1989, Neutrino Astrophysics (Cambridge: Cambridge Univ. Press)
Bahcall, J. N., Bahcall, N. A., & Shaviv, G. 1968, Phys. Rev. Lett., 20, 1209
Bahcall, J. N., & Pinsonneault, M. H. 1991, ApJ, submitted
Bahcall, J. N., & Ulrich, R. K. 1988, Rev. Mod. Phys., 60, 297
Bethe, H. 1939, Phys. Rev., 55, 434
Bodenheimer, P. 1965, ApJ, 142, 451
Böhm-Vitense, E. 1958, Zs. Ap., 46, 108
Chan, K.-L., & Sofia, S. 1989, ApJ, 336, 1022
Christensen-Dalsgaard, J. 1988, in Proc. Symp. Seismology of the Sun and Sun-like Stars, ESA SP-286 (Noordwijk: ESA), 431

Christensen-Dalsgaard, J., Däppen, W., & Lebreton, Y. 1988, Nature, 336, 634
Christensen-Dalsgaard, J., Duvall, T. L., Gough, D. O., Harvey, J. W., & Rhodes, E. J. 1985, Nature, 315, 378
Christensen-Dalsgaard, J., Gough, D. O., & Thompson, M. J. 1991, ApJ, 378, 413
Clayton, D. 1968, Principles of Stellar Evolution and Nucleosynthesis (New York: McGraw-Hill)
Cohen, E. R., & Taylor, B. N. 1986, Codata Bulletin No. 63 (New York: Pergamon Press)
Cox, A. N. 1990, private communication
Cox, A. N., Guzik, J. A., & Kidman, R. B. 1989, ApJ, 342, 1187
Cox, A. N., Guzik, J. A., & Raby, S. 1990, ApJ, 353
Cox, A. N., & Stewart, J. N. 1970, ApJS, 19, 243
Cox, J. P., & Giuli, R. T. 1968, Principles of Stellar Structure (New York: Gordon and Breach), 1327
Däppen, W. 1990, private communication
Däppen, W., & Gough, D. O. 1985, in Seismology of the Sun and the Distant Stars, ed. D. O. Gough (Dordrecht: Reidel), 275
Davis, R., Jr. 1978, in Proc. Informal Conference on Status and Future of Solar Neutrino Research, ed. G. Friedlander, Brookhaven National Laboratory Report 50879, 1, 1
Demarque, P., & Larson, R. B. 1964, ApJ, 140, 544
Demarque, P., & Percy, J. R. 1964, ApJ, 140, 541
Eddington, A. S. 1926, The Internal Constitution of the Stars (Cambridge: Cambridge Univ. Press), 407
Endal, A. S., & Sofia, S. 1981, ApJ, 243, 625
Endal, A. S., Sofia, S., & Twigg, L. W. 1985, ApJ, 290, 748
Fox, P., Theobald, M., & Sofia, S. 1991, ApJ, 383, 860
Fowler, W. A., Caughlan, G. R., & Zimmerman, B. A. 1975, ARA&A, 13, 69
Guenther, D. B. 1989, ApJ, 339, 1156
———. 1991a, ApJ, 369, 247
———. 1991b, ApJ, 375, 352
Guenther, D. B., Jaffe, A., & Demarque, P. 1989, ApJ, 345, 1022
Guenther, D. B., & Sarajedini, A. 1988, ApJ, 327, 993
Hickey, J. R., & Alton, B. M. 1983, in Solar Irradiance Variations of Active Region Time Scales (NASA CP-2310), ed. B. J. LaBonte, G. A. Chapman, H. S. Hudson, & R. C. Wilson (Washington, DC: NASA), 43
Huebner, W. F., Merts, A. L., Magee, N. H., & Argo, M. F. 1977, Los Alamos Scientific Laboratory Report, No. LA-6760-M
Hummer, D. G., & Mihalas, D. 1988, ApJ, 331, 794
Iglesias, C. A., & Rogers, F. J. 1991, ApJ, 371, 408
Jiménez, A., Pallé, P. L., Pérez, J. C., Régulo, C., Roca Cortés, T., Isaak, G. R., McLeod, C. P., & van der Raay, H. B. 1987, in IAU Symp. 123, Advances in Helio- and Asteroseismology, ed. J. Christensen-Dalsgaard & S. Frandsen (Dordrecht: Reidel), 205
Kim, Y.-C., Demarque, P., & Guenther, D. B. 1991, ApJ, 378, 407
Korzennik, S. G., & Ulrich, R. K. 1989, ApJ, 339, 1144
Krishna Swamy, K. S. 1966, ApJ, 145, 174
Kurucz, R. L. 1991, private communication
Landau, E. M., & Lifshitz, E. M. 1959, Statistical Physics (Oxford: Pergamon Press), § 78
Lane, J. H. 1869, AJS, 2d Ser., 50, 452
Libbrecht, K. G., Woodard, M. F., & Kaufman, J. M. 1990, ApJS, 74, 1129
Mihalas, D., Däppen, W., & Hummer, D. G. 1988, ApJ, 331, 815
Mihalas, D., Hummer, D. G., Mihalas, B. W., & Däppen, W. 1991, ApJ, submitted
Mikheyev, S. P., & Smirnov, A. Y. 1986, Nuovo Cimento C, 9, 17
Pallé, P. L., Hernández, F. P., Cortés, T. R., & Isaak, G. R. 1989, A&A, 216, 253
Pinsonneault, M. H. 1988, Ph.D. thesis, Yale University
Pinsonneault, M. H., Kawaler, S. D., & Demarque, P. 1990, ApJS, 74, 501
Pinsonneault, M. H., Kawaler, S. D., Sofia, S., & Demarque, P. 1989, ApJ, 338, 424
Prather, M. 1976, Ph.D. thesis, Yale University
Ross, J. E., & Aller, L. H. 1976, Science, 191, 1223
Sackmann, I.-J., Boothroyd, A. I., & Fowler, W. A. 1990, ApJ, 360, 727
Schwarzschild, M., Howard, R., & Härm, R. 1957, AJ, 125, 233
Sofia, S., Maier, E., & Twigg, L. 1991, Adv. Space Res., 11, 123
Tilton, G. R. 1988, in Meteorites and the Early Solar System, ed. J. F. Kerridge & M. S. Mathews (Tucson: Univ. of Arizona Press), 259
Turck-Chièze, S., Cahen, S., Cassé, M., & Doom, C. 1988, ApJ, 335, 415
Ulrich, R. K., & Rhodes, E. J., Jr. 1977, ApJ, 218, 521
———. 1983, ApJ, 265, 551
Wolfenstein, L. 1978, Phys. Rev. D, 17, 2369